OPEN BIOLOGY

Ninein is essential for apico-basal microtubule formation and CLIP-170 facilitates its redeployment to non-centrosomal Microtubule Organising Centres

Journal:	*Open Biology*
Manuscript ID	RSOB-16-0274.R2
Article Type:	Research
Date Submitted by the Author:	n/a
Complete List of Authors:	Goldspink, Deborah; University of East Anglia, School of Biological Sciences Rookyard, Christopher; University of East Anglia, School of Computing Science Tyrrell, Benjamin; University of East Anglia, School of Biological Sciences Gadsby, Jonathan; University of East Anglia, School of Biological Sciences Perkins, James; University of East Anglia, School of Biological Sciences Lund, Elizabeth ; University of East Anglia, School of Biological Sciences Galjart , Niels; Erasmus MC Thomas, Paul; University of East Anglia, School of Biological Sciences Wileman, Tom; University of East Anglia, Medical School Mogensen, Mette; University of East Anglia, School of Biological Sciences
Subject:	cellular biology, developmental biology, molecular biology
Keywords:	ninein, microtubules, MTOC, CLIP-170, epithelia, organoids

Ninein is essential for apico-basal microtubule formation and CLIP-170 facilitates its redeployment to non-centrosomal Microtubule Organising Centres

Deborah A Goldspink[1], Chris Rookyard[2], Benjamin J Tyrrell[1], Jonathan Gadsby[1], James Perkins[1], Elizabeth K Lund[1], Niels Galjart[4], Paul Thomas[1], Tom Wileman[3] and Mette M Mogensen[1*]

[1] School of Biological Sciences, University of East Anglia, Norwich, UK
[2] School of Computing Science, University of East Anglia, Norwich, UK
[3] Medical School, University of East Anglia, Norwich, UK
[4] Department of Cell Biology and Genetics, Erasmus MC, Rotterdam, The Netherlands

Key words: microtubules, ninein, CLIP-170, IQGAP1, Rac1, epithelial differentiation, non-centrosomal MTOCs, intestine, organoids

*Correspondence to: Mette M Mogensen, School of Biological Sciences, University of East Anglia, Norwich, NR4 7TJ, UK. E-mail: m.mogensen@uea.ac.uk

Abstract

Differentiation of columnar epithelial cells involves a dramatic reorganisation of the microtubules and centrosomal components into an apico-basal array no longer anchored at the centrosome. Instead, the minus-ends of the microtubules become anchored at apical non-centrosomal Microtubule Organising Centres (n-MTOCs). Formation of n-MTOCs is critical as they determine the spatial organisation of microtubules, which in turn influences cell shape and function. However, how they are formed is poorly understood. We have previously shown that the centrosomal anchoring protein ninein is released from the centrosome, moves in a microtubule dependent manner and accumulates at n-MTOCs during epithelial differentiation. Here we report using depletion and knockout approaches that ninein expression is essential for apico-basal array formation and epithelial elongation, and that CLIP-170 is required for its redeployment to n-MTOCs. Functional inhibition also revealed that IQGAP1 and active Rac1 co-ordinate with CLIP-170 to facilitate microtubule plus-end cortical targeting and ninein redeployment. Intestinal tissue and *in vitro* organoids from the *Clip1/Clip2* double knockout mouse with deletions in the genes encoding CLIP-170 and CLIP-115, respectively, confirmed requirement of CLIP-170 for ninein recruitment to n-MTOCs, with possible compensation by other anchoring factors such as $p150^{Glued}$ and CAMSAP2 ensuring apico-basal microtubule formation despite loss of ninein at n-MTOCs.

Introduction

Apico-basal polarisation and differentiation of simple epithelial cells such as those of the kidney and intestine involve not only a dramatic reorganisation of the microtubules (MTs) but also of centrosomal components. The radial MT array focused on a centrally located centrosomal Microtubule Organising Centre (MTOC) found in undifferentiated epithelial cells reorganises during differentiation to form a mainly non-centrosomal apico-basal array with minus-ends directed apically (1-5). In polarised epithelia such as kidney, the minus-ends of the apico-basal MTs become anchored at apical non-centrosomal MTOCs (n-MTOCs) associated with adherens junctions (AJ, zonula adherens) (6). Centrosomal anchoring proteins including ninein relocate to these sites, co-localising with β-catenin and the dynactin component $p150^{Glued}$ (6-8). Analyses of MT reorganisation based on regrowth following Nocodazole removal and live GFP-EB1 imaging in kidney (MDCK) cells have established that the apico-basal MTs originate from the centrosome but the vast majority subsequently become anchored at apical n-MTOCs (6, 9, 10). However, in terminally differentiated intestinal epithelial cells both nucleating and anchoring components are redeployed to apical surface associated n-MTOCs (11, 12). A n-MTOC may thus act either as an anchoring or as a nucleating and anchoring site for non-centrosomal MTs. N-MTOCs are critical as they determine the temporal and spatial MT anchorage and organisation, which in turn influences the shape and function of epithelial cells. However, the mechanisms responsible for MT minus-end anchorage and formation of n-MTOCs are poorly understood.

The importance of the centrosomal protein ninein in development is evident through studies which have shown that it influences neurogenesis, angiogenesis and stem cell fate and *Nin* gene mutations that cause human disorders such as microcephalic primordial dwarfism and spondyloepimetaphyseal dysplasia (13-17). Ninein is a large coiled-coil protein that associates with the subdistal appendages of the mother centriole and the minus-ends of both centrioles (7). Loss- and gain-of-function studies have established that ninein acts as a major MT minus-end anchor at the centrosome but whether this is also the case at n-MTOCs in polarised epithelial cells remains to be established (18, 19). Analyses of *in situ* inner ear epithelial cells revealed that ninein gradually relocates to apical non-centrosomal anchoring sites during inner ear morphogenesis, while live-cell imaging showed that GFP-ninein speckles move to and from the centrosome in a MT dependent manner

(7, 8) (20). Relocation of ninein from the centrosome to cortical sites has also been reported during epidermis differentiation (21). However, the molecular mechanisms responsible for the relocation of ninein during polarised epithelial differentiation still remain to be determined.

MT plus-end tracking proteins (+TIPs) have proved essential for MT reorganisation during differentiation of epithelia and skeletal muscle (22-24). CLIP-170 was the first +TIP characterised (25) and shown to accumulate at MT plus-ends and act as a rescue factor (26). CLIP-170, CLIP-115 and $p150^{Glued}$ bind MTs and EB1 through CAP-Gly domains (27). MT plus-end cortical interactions facilitated by +TIPs have proved important for several cellular processes such as directed cell migration, centrosome repositioning, spindle orientation and adherens and gap junction formation. For example, EB1, dynein/dynactin and CLIP-170 mediate MT cortical capture at the leading edge of migrating cells and at adherens junctions (AJs), with CLIP-170 shown to target AJs prior to apico-basal array assembly (6, 28-30). MT plus-end cortical interactions and CLIP-170 may thus facilitate delivery of ninein to n-MTOCs and promote the formation of non-centrosomal apico-basal MT arrays in differentiating epithelial cells. The main focus of this investigation was therefore to determine whether CLIP-170 is required for redeployment of ninein to n-MTOCs during epithelial differentiation. Additionally, the involvement of active Rac1 and the cortical receptor IQGAP1 was also explored, as these two proteins have been shown to interact with CLIP-170, form a complex and capture MT plus-ends at the cortex (31).

Here we show that ninein expression is essential for apico-basal MT formation and columnar epithelial shape. We also show that ninein and CLIP-170 localise to apical junction associated n-MTOCs in fully differentiated MDCKII cysts and apical surface n-MTOCs in terminally differentiated (villus) epithelial cells of *ex-vivo* intestine and *in vitro* organoids generated from mouse small intestine. We also identify $p150^{Glued}$, γ-tubulin and CAMSAP2 (calmodulin-regulated spectrin-associated protein 2) at the n-MTOCs in villus tissue and organoids. Using *in vitro* and *ex-vivo* depletion and knockout (KO) studies we show that CLIP-170, IQGAP1 and active Rac1 influence MT plus-ends cortical contact and facilitate redeployment of ninein to apical n-MTOCs. We propose a model for ninein redeployment in which dynamic CLIP-170 bound MT plus-ends target and are captured by IQGAP1 cortical receptors in a process promoted by active Rac1. In addition, the *Clip1/Clip2* double

KO mouse with deletions in the genes encoding CLIP-170 and CLIP-115, respectively, confirmed the requirement of CLIP-170 for ninein recruitment to n-MTOCs and suggests engagement of a compensation mechanism to ensure non-centrosomal apico-basal MT formation in the absence of CLIP-170 and ninein at n-MTOCs.

Results

Ninein siRNA depletion inhibits apico-basal microtubule bundle formation and epithelia cell elongation.

Although ninein is needed for centrosomal MT anchorage, its role in apico-basal MT array formation is not known. Human TC7 colonic cells, which readily elongate and produce 10–12μm tall cells with apico-basal arrays when grown to confluence, were used as a model to investigate the role of ninein in apico-basal MT array formation (22). Ninein siRNA depletion was performed using previously tested sequences (8, 15), which as expected (19) produced loss of centrosomal anchorage and disorganised MTs in non-confluent epithelial cells (Fig.1A,B).

In confluent TC7 cells a typical apico-basal epithelial MT organisation was evident in scramble-siRNA cells, with lateral views showing apico-basal alignment of MTs and cross-sections revealing peripheral MT rings representing optical cross-sections of the apico-basal array (Fig.1C). However, ninein knockdown revealed a striking lack of cell elongation and apico-basal MTs with optical cross-sections through the middle region, instead showing disorganised networks within 3-fold larger cells (Fig.1C,D). These findings show that ninein expression is critical for apico-basal MT array formation and epithelial elongation.

Ninein and CLIP-170 localise to apical n-MTOCs in 3D MDCKII cysts and are part of the membrane fraction.

Cortical ninein and CLIP-170 have previously been identified and localised in 2D *in vitro* confluent and polarised MDCKII cell layers and this cell model was therefore used for further analysis of junction-associated n-MTOCs (6, 8, 32). Here we show 3D MDCKII cysts grown in Matrigel with differentiated epithelial cells possessing distinct apico-basal MT arrays, apical centrosomes and ninein and CLIP-170 at apical junction associated n-MTOCs (Fig.2A,B). An apical peripheral ring of ninein and CLIP-170 is evident which co-localises with the minus-ends of the apico-basal MTs (Fig.2Aii;Biv). CLIP-170 comets and ninein speckles are also present in the cytoplasm and ninein is evident at the apical centrosome while γ-tubulin is present at the centrosome but absent from the n-MTOCs (Fig.2Aii;Aiii,Bi;Bii).

Some co-localisation of ninein and CLIP-170 was evident in confluent MDCKII cells, however, co-immunoprecipitation did not reveal any complex formation between ninein and CLIP-170 (Fig.2C and data not shown). Expression of GFP-CLIP-170 also revealed accumulation at the cell cortex and cell fractionation confirmed endogenous CLIP-170 within the membrane and cytosolic fractions (Fig.2D,E). Nocodazole treatment to depolymerise MTs revealed both endogenous and GFP-CLIP-170 remained at the cortex and that CLIP-170 was still in the membrane fraction (Fig.2D,E). Similarly, cortical ninein remained at the cortex in the presence of Nocodazole (Fig.2F). Interestingly, a proteomics study has also identified ninein and CLIP-170 in the membrane fraction of U20S cells (peptracker.com) (33). This suggests that both ninein and CLIP-170 are associated with the cortex and that they are bound there independently of MTs.

Differentiated intestinal epithelia and organoids show accumulation of ninein and CLIP-170 at apical surface n-MTOCs.

Although the 2D and 3D *in vitro* epithelial cultures show that a fraction of CLIP-170 and ninein localise to apical cortical n-MTOC during differentiation, it is important to determine whether this is the case *in vivo* and if this is linked to differentiation. The intestinal epithelium is a good model to investigate the redeployment of ninein during differentiation as it contains both proliferating and differentiated epithelial cells. A hierarchy of differentiation is evident in the small intestine. Stem cells at the bottom of crypts give rise to immature transit-amplifying cells that proliferate and gradually differentiate as they migrate up the crypt into the villus, where they become fully differentiated enterocytes prior to being shed into the lumen (34) (Fig.3C). The stem cell niche at the bottom of the crypts thus contain undifferentiated while the upper villus contains terminally differentiated epithelial cells.

In the stem cell region of the crypts ninein was concentrated at the apical centrosome, where it co-localised with γ-tubulin, while CLIP-170 comets were evident throughout the cytoplasm (Fig.3A). No discernable accumulation of ninein or CLIP-170 was apparent at apical cortical sites. In contrast, terminally differentiated villus cells, which lack centrosomes and have γ-tubulin at the apical surface (11, 35) revealed distinct apical bands of both ninein and CLIP-170 at the

apical surface and at junctions (Fig.3B). Ninein and CLIP-170 were present not only at the AJs (Fig.3Biv,v) but also just below the apical surface (Fig.3Bii;vi). CLIP-170 was also present along the lattice of the apico-basal MTs (Fig.3Bvi). Fully differentiated epithelial cells of the villus thus exhibited distinct non-centrosomal apico-basal MT bundles with minus-ends anchored within apical n-MTOCs containing ninein and CLIP-170.

In vitro gut organoids also referred to as “mini-guts” are reported to mimic the architecture and morphogenesis of the *in vivo* gut but whether this includes centrosomal reorganisation during differentiation has not been established. Here we generated gut organoids from mouse small intestine as previously described (36) (Fig. 3C). Cells from the stem cell niche proliferate forming aggregates and cysts that subsequently generate crypt-like buds with stem cells at the base and differentiation gradually progressing towards the cyst region, which become villus-like (Fig.3C; S1). Apico-basal MT arrays, which form during gut organoid development, were evident in cells of both the proliferating stem cell niche (base of crypts) and fully differentiated villus domains (Fig.3D). However, as for the *ex-vivo* tissue data, ninein was concentrated at the centrosome in crypt/stem cells (Fig.3Di) while both ninein and CLIP-170 localised at the apical n-MTOC in cells of the organoid villus domains (Fig.3Dii,iii).

CLIP-170 siRNA knockdown in MDCKII cells reveal marked reduction in cortical ninein and reduced cyst size.

In order to determine whether CLIP-170 affects cortical localisation of ninein it was knocked down using siRNA in MDCKII cells, which as previously described show distinct cortical n-MTOC ninein when confluent (partially polarised) (Fig.2C). Four CLIP-170 siRNA predicted sequences (a-d) were tested, with Western blot analysis showing most efficient knockdown with sequence d (Fig.4A). Confluent scramble-siRNA control cells showed ninein at the centrosome, as speckles in the cytoplasm and at the cortex. However, CLIP-170 siRNA knockdown resulted in a marked reduction in cortical ninein (Fig.4B). Average fluorescence intensity profiles through cell-cell junctions resulted in a 57% reduction in junctional ninein in CLIP-170 knockdown cells (Fig.4C,D). Importantly, no differences in overall ninein protein levels or centrosome fluorescence intensity were observed between scramble and

CLIP-170 siRNA-treated cells showing that ninein expression and its dynamic exchange at the centrosome (8) had not been affected (Fig.4E,F).

Both scramble and CLIP-170 siRNA knockdown MDCKII cells formed 3D cysts with a central lumen and polarised cells (Fig.4G). However, CLIP-170 knockdown resulted in markedly smaller cysts with 38.6% smaller cross-sectional area compared to scramble cysts (Fig.4H).

Clip1/Clip2 double knockout mouse intestine and organoids reveal abnormalities.

The *in vitro* knockdown data suggested that CLIP-170 is required for efficient location of ninein to apical cortical n-MTOCs. The effect of lack of CLIP-170 was therefore investigated further *in ex-vivo* intestinal tissue of the *Clip1/Clip2* double KO mouse in which the genes encoding CLIP-170 and CLIP-115, respectively, have been deleted (Fig.5A). Although epithelia predominantly express CLIP-170, the double KO was used to prevent possible compensation by CLIP-115. *Clip1/Clip2* double KO mice survive and the gross small intestinal morphology based on tissue sections appeared normal with the villus and crypts containing columnar epithelial cells (Fig.S2). However, some developmental abnormalities were observed in both *ex-vivo* tissue and *in vitro* organoids of the *Clip1/2* double KO.

Epithelial cells with basal located nuclei and apico-basal MTs were evident in both crypt and villus tissue of the double KO (Figs.5B,6A;S2). However, the apical polarity marker gp135 (podocalyxin) located more sparsely at the apical surface of villus cells in the KO compared to WT (Figs.5B;S3). Interestingly, in contrast to the WT, terminally differentiated KO villus cells retained their centrioles, suggesting that centriolar disassembly is affected in KO intestine (Fig.5C). In addition, less acetylated MTs were apparent in the KO compared to WT villus cells (Fig.S4).

Organoids were successfully generated from the small intestine of the *Clip1/2* double KO but lack of CLIP-170/115 led to delayed development. Formation of buds that developed into crypts was significantly reduced in KO cultures compared to WT. There was a 43.5% increase in cysts with no buds and 75.9% fewer organoids with 4 or more buds in the KO compared to WT cultures by day 6 (Fig.5D,E).

These findings suggest that although CLIP-170 is not essential for gut epithelial formation, it does appear to be required for efficient apical positioning of gp135, disassembly of the centrioles, maintenance of a population of acetylated MTs in terminally differentiated villus cells and for efficient organoid development.

Intestinal epithelial cells from the *Clip1/Clip2* double knockout mouse lack ninein at apical n-MTOCs.

Strikingly, almost complete absence of apical cortical ninein was evident throughout the small intestine of the *Clip1/2* double KO. Baso-lateral views of villus cells in the KO revealed a lack of apical cortical ninein, which was prominent in the WT (Fig.6A, upper panels) with apical cross-sections of the villus emphasising the almost complete absence of ninein at the junctions (Fig.6A, lower panel). Fluorescence intensity profiles through apical junctions showed an 86% reduction in ninein in the KO villus cells compared with the WT, while no change in β-catenin intensity confirmed the junctions were intact (Fig.6B,C).

γ-Tubulin is known to relocate to the apical surface n-MTOC in fully differentiated epithelial cells of the villus (11). Interestingly, γ-tubulin showed similar apical surface location in KO to WT despite lack of ninein and CLIP-170 at the n-MTOCs with fluorescence intensity analysis revealing no significant difference (Fig.6D and data not shown). These results suggest that CLIP-170 is required for ninein but not γ-tubulin deployment to apical n-MTOCs during intestinal epithelial differentiation. In addition, it shows that γ-tubulin is not dependent on ninein for its localisation at the apical surface n-MTOCs.

CLIP-170 siRNA depletion leads to reduced microtubule cortical targeting

The CLIP-170 siRNA knockdown in MDCKII cells and *Clip1/2* KO mouse data revealed significant reductions in apical cortical ninein suggesting that CLIP-170 is required for ninein deployment to n-MTOCs. This may be due to CLIP-170 facilitating MT plus-end cortical capture ensuring efficient delivery of ninein along MTs and/or due to cortical CLIP-170 recruiting ninein through cytoplasmic diffusion. We first determined whether MTs were involved in ninein redeployment to n-MTOCs. We established using a Nocodazole assay and fluorescence intensity analysis that less cortical ninein was evident in confluent MDCKII cells following MT

depolymerisation while MT regrowth following Nocodazole removal restored cortical ninein to control levels (data not shown). This suggests that MTs are required for efficient ninein localisation to n-MTOCs. We then tested whether MT plus-end cortical targeting mediated by CLIP-170 is involved in ninein redeployment by siRNA depletion of CLIP-170 in human retinal pigmented epithelial cells (ARPE-19). ARPE-19 cells were chosen as they contain distinct radial arrays with MTs approaching the cortex perpendicularly and any deviations from this pattern can easily be detected (6). CLIP-170 localised as comets or elongated rods at plus-ends, and as puncta along the MT lattice in ARPE-19 cells (Fig.7A). Two different siRNA sequences against human CLIP-170 were used both showing complete loss of CLIP-170 expression and no off-target effects on EB1 expression (Figs.7B,S5).

To better compare MT organisation, mixed ARPE-19 cell cultures containing both depleted and scramble siRNA-treated cells were used. Cells were treated separately with either scramble or CLIP-170 siRNA and then mixed 24 hours prior to immuno-labelling. In the vast majority of CLIP-170 depleted cells MTs had lost radial organisation, centrosomal focus and perpendicular cortical approach (Fig.7C). Many MTs appeared disorganised, forming a criss-cross pattern with several MTs aligned parallel to the cortex (Fig.7C,D). To determine if CLIP-170 has a role in MT cortical targeting, perpendicular MT approach to the cortex was assessed blind in control, scramble and CLIP-170 siRNA treated cells. Analyses showed a significant reduction in perpendicular MTs in CLIP-170-depleted compared to control/scramble cells (Fig.7E). This could be rescued with GFP-rat-CLIP-170 that is not targeted by the siRNAs (Fig.7E,F). MT cortical targeting was further assessed using a Nocodazole regrowth assay in mixed cultures. MTs had fully recovered a radial array with perpendicular cortical approach 30 mins following Nocodazole washout in control and scramble siRNA cells whereas CLIP-170 depleted cells had not (Fig.7G,H). Again this could be rescued with GFP-rat-CLIP-170 (Fig.7G). This was also observed with CLIP-170 siRNA sequence 2 in U2OS cells (data not shown). These results suggest that MT cortical targeting is compromised in cells lacking CLIP-170 and this is likely to contribute to the reduced cortical ninein.

IQGAP1 acts as a cortical receptor for CLIP-170 and its knockdown leads to reduced cortical ninein.

The cortical receptor and Rac1/Cdc42 effector IQGAP1 has been shown to interact with CLIP-170 and to capture and stabilise MTs at the cell cortex in migrating cells (31). However, its role in MT capture at cell junctions has not been investigated. Here we show that IQGAP1 co-immunoprecipitated with CLIP-170 in confluent human intestinal TC7 cells suggesting that these proteins also interact in non-migrating epithelial cells (Fig.8A). In addition, the CLIP-170 IP also pulled down the AJ component β-catenin (Fig.8A), which has also been reported to interact with IQGAP1 (37).

IQGAP1 localised to the inner face of β-catenin puncta at cell-cell contacts in ARPE-19, MDCKII, HeLa, TC7 and U2OS epithelial cells with MTs directly targeting IQGAP1/β-catenin clusters (Fig.8B and data not shown). Nocodazole recovery assays in ARPE-19 cells showed re-forming MTs positive for CLIP-170 target cortical IQGAP1 at cell-cell junctions (Fig.8Bii). IQGAP1 may thus act as a cortical receptor at AJs for the capture of CLIP-170 bound MTs, and facilitate ninein relocation. Depletion of IQGAP1 in ARPE-19 cells produced similar results to CLIP-170, with a significant reduction in MT perpendicular approach, suggesting that IQGAP1 influences MT plus-end targeting/capture (Figs.7E;8C).

Previously, IQGAP1 expression has been linked to junction integrity, which in turn could affect cortical ninein accumulation (38). Maintenance of junction integrity was confirmed by IQGAP1 knockdown in MDCKII cells, with fluorescence intensity profiles through cell junctions revealing no change in β-catenin (Fig.8G). However, a marked loss in cortical ninein was evident in IQGAP1 siRNA treated cells with junctional fluorescence intensity profiles showing a 74% reduction in ninein (Fig.8E-G) despite the total ninein protein level remaining the same (Fig.4E). This suggests that IQGAP1 coordinates with CLIP-170 to mediate MT cortical targeting and capture to facilitate ninein redeployment.

Rac1 inhibition affects MT dynamics and cortical targeting and leads to reduced cortical ninein.

Active Rac1 has been reported to promote CLIP-170 and IQGAP1 complex formation and to facilitate and prolong MT cortical capture in migrating cells, with active Rac1 promoting MT growth into lamellipodia (31, 39). However, the effect of

Rac1 on MT organisation and dynamics in confluent epithelial cells is not known and was therefore investigated with regard to ninein redeployment.

Rac1 was evident at AJs in MDCKII and APRE-19 cells co-localising with β-catenin, IQGAP1 and ninein (Figs.S6A). Interestingly, Rac1 aligned along MTs in some junctional regions (Fig.S6B). Rac1 was inhibited with NSC23766, a specific inhibitor of Rac1-GEF interaction that prevents Rac1 activation (40). Loss of peripheral actin arcs and dorsal stress fibres (perpendicular actin bundles) and an increase in ventral stress fibres in NSC23766 treated cells confirmed effective Rac1 inhibition (Fig.S6C). The effect of Rac1 inhibition on ninein redeployment was investigated in MDCKII cells. Cells treated with NSC23766 showed 84% reduction in cortical ninein compared to control cells (Fig.9A-C). Fluorescence intensity profiles of E-cadherin confirmed maintenance of junction integrity and showed unchanged centrosomal ninein and protein levels in Rac1-inhibited cells (Figs.4E,F;9C). Reduced cortical ninein in Rac1-inhibited cells suggests that active Rac1 promotes efficient ninein delivery and that MT cortical targeting and dynamics may be affected by Rac1 inhibition.

Rac1 inhibition in confluent ARPE-19 cells maintained centrosome focused MT arrays but resulted in extensive looping around the cell periphery (Fig.9D). To quantify MT cortical targeting and approach, the relative orientation of MTs to cell junctions was assessed using the ImageJ (FIJI) plugin “FibrilTool” (41). In control cells the MTs were on average orientated at 54° to the cell junctions, which was reduced to 10° in Rac1-inhibited cells, confirming a close to parallel orientation (Fig.9E). Analysis of MT cortical contact, assessed by counting the number of contacts per 10μm of junction, revealed on average 6 MT contacts in control cells but only 3 in Rac1-inhibited cells (Fig.9F). These data suggest that active Rac1 is required for cortical MT targeting and contact at cell junctions.

To assess the affect of Rac1 inhibition on MT dynamics the number of CLIP-170 comets was analysed. Rac1 inhibition led to significantly fewer CLIP-170 comets (Fig.10A,B). MT dynamic behavior was further studied in ARPE-19 cells expressing GFP-CLIP-170 by live time-lapse image analysis using the automated tracking software U-Track, originally plusTipTracker (42). It should be noted that stabilised MTs will generally not be detected by this method and the addition of GFP-CLIP-170 may promote some MT rescue. GFP-CLIP-170 comet analysis showed more growth and fewer pausing events in Rac1-inhibited cells compared to

control cells (Fig.10C,D; Supplementary movies1,2). However, the phases of growth were shorter and the average comet velocity was lower in Rac1-inhibited (6.3μm/min) compared to control (12.1μm/min) cells (Fig.10E,F). To further analyse the differences in growth, the data was divided into 4 speed groups and the distributions for each treatment was studied. The Rac1-inhibited cells showed a different distribution of comet speeds with reduced fast and very fast comets but increased percentages of very slow comets (Fig.10G). This suggests that active Rac1 encourages fast persistent MT growth to the AJs and initiates MT capture by promoting pausing.

Apico-basal microtubule arrays are maintained in the absence of ninein at n-MTOCs.

Here we have shown that ninein expression is essential for apico-basal microtubule formation and epithelial elongation and that ninein recruitment to apical n-MTOCs is dependent on CLIP-170 and its co-ordination with IQGAP1 and active Rac1. However, apico-basal MT organisation was evident in villus cells of both *ex-vivo* intestinal tissue and *in vitro* organoids of the KO as well as in CLIP-170 knockdown MDCKII cysts (Fig.4G;11A). Note that ninein is present at the centrosome and as speckles in the cytoplasm in both KO and knockdown cells and the level of its expression is unchanged (Fig.4E). The presence of apico-basal MTs despite lack of ninein at the apical n-MTOCs in knockdown/KO epithelial cells reveal that ninein is not essential for apico-basal array maintenance and suggests that it is not essential for MT minus-end anchorage at n-MTOCs and that other proteins/complexes compensate. Indeed, the dynactin subunit $p150^{Glued}$, which has been reported to have a role in MT minus-end anchorage at the centrosome (43), was evident at the apical n-MTOCs in both WT and KO villus cells (Fig.11B,C). Cross-sections of villus cells revealed $p150^{Glued}$ puncta at apical junctions and surfaces in both KO and WT while lateral views indicated MT minus-ends within apical $p150^{Glued}$ puncta (Figs.11B,C). Most interesting, CAMSAP2, a member of the novel calmodulin-regulated spectrin-associated protein family, which binds and stabilise the minus-ends of non-centrosomal MTs (44-47), was also evident at apical n-MTOCs in WT villus tissue co-localising with $p150^{Glued}$ (Fig.S7). Furthermore, CAMSAP2 was present at apical n-MTOCs in *in vitro* organoids generated from both WT and KO small intestine (Fig.11D).

The results reveal that although ninein expression is required for apico-basal MT formation and epithelial polarisation its localisation at n-MTOCs is not essential for maintenance of the apico-basal array. Furthermore, the findings show that CLIP-170 is required for ninein but not γ-tubulin, $p150^{Glued}$ or CAMSAP2 deployment to apical n-MTOCs during intestinal epithelial differentiation.

Discussion

How the centrosome reorganises its components and n-MTOCs form are poorly understood and yet n-MTOCs are critical for apico-basal epithelial differentiation as they determine MT positioning, which underpins cell shape and function (4, 48, 49). Here we show using both *in vitro* siRNA depletion and *ex-vivo* mouse knockout studies that CLIP-170 is required for redeployment of the MT minus-end anchoring protein ninein to n-MTOCs but not for γ-tubulin. The data suggest that CLIP-170 together with IQGAP1 and Rac1 form a complex at AJs that facilitates ninein relocation to n-MTOCs during differentiation. Loss of CLIP-170 delayed development of 3D epithelial and mouse organoid cultures, although lack of ninein at n-MTOCs did not prevent the formation and maintenance of apico-basal arrays. Interestingly, $p150^{Glued}$ and the novel MT minus-end stabiliser CAMSAP2 maintained their location at n-MTOCs in *Clip1/Clip2* double KO organoids, and may compensate for the lack of ninein. In addition, although ninein is able to bind γ-tubulin (20), the KO data revealed that γ-tubulin is not dependent on ninein for its localisation at apical surface n-MTOCs. This is also the case for C. elegans where γ-tubulin is recruited to n-MTOCs independently of the ninein-related protein NOCA-1 (50).

A defining step in epithelial differentiation is the accumulation of anchoring proteins such as ninein at apical n-MTOCs while centrosomal MT anchorage diminishes (8). The present study showed that fully differentiated epithelial cells in cysts and small intestinal *ex-vivo* tissue and *in vitro* organoids possess ninein and CLIP-170 at n-MTOCs, which are associated with AJs in MDCKII and with both AJs and the apical surface in intestinal villus cells. In contrast, in proliferating cells located in the stem cell region at the bottom of the intestinal crypts ninein was concentrated at the apical centrosome while CLIP-170 was present as MT plus-end comets in the cytoplasm. We have previously established that ninein is highly dynamic, moves in and out of the centrosome in a MT dependent manner (8) and here we further show that MTs are required for ninein redeployment to n-MTOCs. In addition, Nocodazole assays and ultrastructural analyses have suggested that initial MT plus-end targeting followed by minus-end anchorage at AJs are important steps in the generation of non-centrosomal apico-basal MTs (6). In the present study,

depletion or inhibition of CLIP-170, IQGAP1 or Rac1 caused compromised MT cortical targeting and a dramatic reduction in ninein location at n-MTOCs.

Both CLIP-170 and EB1 have been implicated in MT cortical targeting for adherens and gap junction formation (29, 30). Here we have shown that CLIP-170 bound MT plus-ends target IQGAP1 puncta on the inner face of β-catenin at cell-cell contacts with their interaction confirmed by Co-IP. The localisation of IQGAP1 at AJs is likely to be mediated through its binding to β-catenin, E/N-cadherin, active Rac1 or F-actin (37, 51, 52). IQGAP1 is thus ideally positioned at AJs to capture MT plus ends via CLIP-170, although β-catenin has also been identified as an interactor of CLIP-170 and may act as an alternative cortical receptor. Depletion of either CLIP-170 or IQGAP1 resulted in loss of MT cortical targeting as well as a significant reduction in cortical ninein. The importance of CLIP-170 in ninein redeployment during epithelial differentiation was also verified in *ex-vivo* intestinal tissue and organoids of the *Clip1/Clip2* double KO mouse, which lack CLIP-170 and CLIP-115 and fail to locate ninein to n-MTOCs.

Rac1 inhibition resulted in fewer CLIP-170 comets, increased MT stability, compromised cortical targeting and a significant reduction in cortical ninein. This fits with other studies where Rac1 inhibition has been shown to suppress MT dynamics and targeted growth as for example in fibroblasts (53). In endothelial cells, active Rac1 is required for IQGAP1, EB1 and cortactin complex formation, and MT cortical capture (54). A more detailed analysis of MT dynamics using live GFP-CLIP-170 imaging and U-Track revealed more growth and fewer pausing events, with a significant reduction in fast comets in inhibited compared with control cells. This suggests that active Rac1 facilitates ninein relocation by promoting fast persistent MT growth towards AJs, with increased pausing enabling capture at these sites. Interestingly, RNAi knockdown of EB1 in epithelial cells, using a previously characterised EB1 shRNA (24), had no effect on cortical ninein relocation (data not shown) suggesting that specific +TIP capturing complexes are required for ninein redeployment.

We propose two alternative but not mutually exclusive models for ninein redeployment to n-MTOCs. In the first model, dynamic CLIP-170 bound MT plus-ends, target and are captured by IQGAP1 at apical AJ associated n-MTOCs in a process promoted by active Rac1. Here CLIP-170 acts as a +TIP facilitating MT cortical targeting and ninein delivery along MTs to the n-MTOCs. Loss of CLIP-170,

IQGAP1 or active Rac1 results in compromised MT cortical targeting/capture and ninein delivery to n-MTOCs. In the second model CLIP-170 together with IQGAP1 and active Rac1 act as a cortical receptor/anchoring complex for ninein at n-MTOCs with loss of CLIP-170, IQGAP1 or active Rac1 resulting in defective ninein recruitment to the n-MTOCs. Future dynamic analyses of MTs and ninein will be needed to determine the exact mechanism by which ninein is localised to n-MTOCs (Fig.12)

It is well established that ninein is essential for MT minus-end anchorage at the centrosome but its role in formation and maintenance of non-centrosomal apico-basal MT arrays had not been investigated (19, 55). Here we show for the first time that expression of ninein and most likely its presence at the centrosome and/or in the cytoplasm as speckles is required for apico-basal array formation and columnar epithelial differentiation. Similarly, the ninein-related protein NOCA-1 in *C. elegans* has also been found to be required for assembly of non-centrosomal MT arrays in epithelial cells (50). Lack of ninein maintained the undifferentiated epithelial phenotype of relatively flat cells with disorganised MT networks. The centrosomal protein CAP350 has also been reported to influences apico-basal MT organisation and epithelial elongation. However, CAP350 does not localise to the apical n-MTOCs but to baso-lateral junctions and assist MT bundle formation by facilitating MT adherens junction interactions (56, 57).

Interestingly, knockdown of CLIP-170 or loss of *Clip1/2* gene expression did cause noticeable developmental abnormalities including reduced cyst size and delayed gut organoid development. In particular, less efficient apical distribution of the transmembrane glycoprotein and polarity marker gp135 (podocalyxin) and fewer acetylated MTs suggest that apical transport and MT stability are affected in the KO and this is likely to be linked to lack of CLIP-170. MTs play an important role in the delivery of gp135, while binding of CLIP-170 along the MT lattice as observed in WT villus cells has been linked to increased MT stability and tubulin acetylation in other cell types (58-62). Interestingly, centriole disassembly is also affected and future analysis will be needed to determine whether CLIP-170 and/or ninein redeployment play a role.

Surprisingly, anchorage of apico-basal MTs at n-MTOCs in differentiated epithelial cells is not dependent on ninein or CLIP-170 as knockdown of CLIP-170 in cells and KO of the *Clip1/2* genes in mouse intestine prevented ninein

localisation to n-MTOCs but not epithelial elongation or apico-basal MT formation and maintenance. Loss of desmoplakin in the villus has also been reported to affect apical ninein localisation without affecting the formation of columnar epithelial cells or apico-basal MT arrays (63). This suggests that other anchoring proteins compensate for lack of ninein at n-MTOCs. Indeed, $p150^{Glued}$, which has been implicated in centrosomal anchoring (43), remained at the n-MTOCs in KO villus cells. Most interesting, CAMSAP2, a member of the novel calmodulin-regulated spectrin-associated protein family, which binds and stabilises the minus-ends of non-centrosomal MTs was evident at apical n-MTOCs in *ex-vivo* intestinal villus tissue (44, 47, 64, 65). Furthermore, CAMSAP2 also localised to n-MTOCs in organoids generated from both WT and *Clip1/2* double KO small intestine and thus in the presence or absence of ninein and CLIP-170 at the n-MTOCs. CAMSAP3 has recently been identified as important for tethering MTs to the apical cortex in intestinal cells with depletion or mutations disrupting MT organisation although without loss of overall apico-basal orientation (66). However, loss of either CAMSAP2 or CAMSAP3 has no effect on formation of polarised intestinal epithelial cysts in 3D culture although loss of non-centrosomal MTs are apparent in CAMSAP3 but not CAMSAP2 knockout cells in 2D polarising cultures (67). Taken together this suggests that the minus-ends of apico-basal MTs are anchored to n-MTOCs by multiple complexes, with loss of ninein from the n-MTOCs compensated for by others such as CAMSAPs. This is particularly interesting as in C. elegans the ninein homologue NOCA-1 functions redundantly with PTRN-1 (CAMSAP homologue) in the assembly of non-centrosomal MT arrays in some tissues (50). It therefore seems likely that both MT minus-end anchoring proteins such as ninein and stabilising proteins such as the CAMSAPs co-operate and are recruited to n-MTOCs to maintain non-centrosomal MT arrays. Proteins that act as platforms for the recruitment of MT minus-end nucleating and/or anchoring/stabilising proteins are also likely to be important for assembly of n-MTOCs. Here our data suggest that IQGAP1/Rac1 and CLIP-170 act as a platform at apical AJs for the recruitment of ninein and formation of anchoring n-MTOCs in differentiating kidney epithelial cells (MDCKII). Interestingly, the spectraplakin ACF7 (MACF1) has recently emerged as critical for the recruitment of CAMSAP3 bound MTs to apical surface n-MTOCs and for formation of polarised intestinal epithelial cysts (67). In *Drosophila* the homologue of ACF7, Shortstop (Shot) and Patronin (CAMSAP homologue) localise

to apical domains together with spectrin and cooperate to generate MT array (68). Further studies will be required to determine the exact role and interplay of these components in non-centrosomal MT minus-end anchorage at n-MTOCs.

Materials and Methods

Clip1/Clip2 double knockout mouse

Generation of the *Clip1/Clip2* double KO mouse strain will be described elsewhere. Briefly, the genes encoding CLIP-170 (*Clip1*) and CLIP-115 (*Clip2*) were targeted as described (58, 69). The *Clip1* gene was subsequently further modified in embryonic stem cells to obtain a completely deleted gene. *Clip1* and *Clip2* single KO mice were then crossed to generate the double knock-out line. Mice were maintained on a C57Bl6 background by crossing heterozygous double knockout mice with wild type C57Bl6 animals (obtained from Harlan, NL). To obtain homozygous double knockout mice for actual experiments, heterozygous male and female mice were mated, and the F1 offspring used. The wild type mice used in these studies were all littermates of the homozygous knockout animals and at P40-80. Experimental procedures and protocols to maintain mouse lines were performed according to the institutional license guidelines.

Cell culture and drug treatment

ARPE-19 (Human Retinal Pigment Epithelial) cells were cultured in DMEM/F12 (Invitrogen) medium supplemented with 10% FBS (Invitrogen), 1% L-glutamine (Invitrogen) and 2% sodium bicarbonate (Invitrogen) at 37°C in 5% CO_2. U2OS (Human Osteosarcoma), TC7 (Human colorectal carcinoma) and MDCKII (Madin-Darby Canine Kidney) cells were cultured in DMEM (Invitrogen) containing 10% FBS, 1% L-glutamine and 0.1 mg/ml streptomycin and 100units/ml penicillin. MCDKII cells were seeded in Matrigel (Corning) and grown for 6 days for 3D cyst experiments.

Nocodazole assays were performed as previously described (6). Inhibition of Rac1 activation was performed using the chemical inhibitor NSC23766 (Tocris; effectiveness between 10μM–1000 μM, (40)). For Rac1 inhibition confluent ARPE-19 and MDCKII cells were treated with 250μM NSC23766 for 12 or 24 hours respectively.

Organoids from WT and KO mice were established as previously described (36) and both were maintained for 3+months in culture. For budding experiments organoids were digested with typLe express (Invitrogen) for 3mins at 37ºC and

fragmented by pipetting. These fragments were then seeded in Matrigel and maintained under normal organoid culturing conditions (36).

Immunolabelling and antibodies

Fixation and immunolabelling of cultured cells were performed as previously described (6). Small intestine was isolated and fractioned as previously described (22, 70, 71). Isolated fractions were fixed in cold -20°C methanol or formaldehyde (9%) / methanol for 10 mins and stained as above. Organoid and cyst were fixed either in their Matrigel setting or following extraction by Cell Recovery Solution (Corning) and then subsequently immuno-stained as previously described (22).

Rabbit polyclonal antibodies against β-catenin (Sigma) were used at 1:2000, ninein Pep3 (8) at 1:1000, CAMSAP2 (CAMSAP1L1, Proteintech) at 1:500 and α-tubulin (Abcam ab15246), IQGAP1 H-109 (Santa Cruz), ninein N5 (Abcam ab52473) and CLIP-170 2360 (72) at 1:200. Mouse monoclonal antibodies against β-catenin (BD biosciences) and γ-tubulin (Abcam ab11316) were used at 1:1000, E-cadherin (BD Biosciences) at 1:500, IQGAP1 (BD Biosciences), Rac1 (BD Biosciences), $p150^{Glued}$ (BD Biosciences), dynein intermediate chain 70.1 (Sigma) and acetylated tubulin (Sigma) at 1:200 and CLIP-170 F3 (Santa Cruz) at 1:50. Rat monoclonal antibodies against tyrosinated tubulin clone YL1/2 (Abcam ab6160) and GP135/Podocalyxin (R&D Systems mab1556) were used at 1:1000 and 1:50, respectively. Secondary antibodies conjugated to Alexa-Fluor 488, 568, or 647 (Invitrogen) were used at 1:1000 and DAPI (Sigma) at 1:2000. Highly cross-absorbed secondary antibodies conjugated to Dylight-488 and 647 (Jackson) were used at 1:800. Phalloidin conjugated to Alexa-488 (Invitrogen) was used at 1:200 for labelling of actin filaments.

siRNA and cDNA transfection

ARPE-19 and U2OS cells were treated with 27nM of siRNA (Qiagen) delivered by Oligofectamine (Invitrogen) as per manufacturers protocol at 0 hours and again at 48 hours, with experiments performed at 96 hours. Mixed cultures were generated by passaging cells at 72 hours and mixing siRNA-treated with scramble, or untreated control cells, and then seeding them onto coverslips. For siRNA knockdown in MDCKII cells ($1X10^6$) 200pmol of siRNA was delivered using Amaxa (Lonza) electroporation programme A-23 at 0 hours and again at 48 hours.

At 60 hrs cells were seeded confluent ($0.3x10^6$ cells per 10mm coverslip) then lysed or immunostained at 96 hours. TC7 cell depletion in polarised cells was performed and analysed as previously described (22).

Allstars scramble-siRNA (Allstar, Qiagen) was used for all siRNA negative controls. Human ninein target sequences; seq a. GCCAGGGTTAGTAATGTCTTCTTGT (15), seq. 2 CGGTACAATGAGTGTAGAA (8), seq. 3 GGAAGACCTAAGAAATGTA (8). Human CLIP-170 target sequences; seq. 1 CCCGACCTTCAAAGTTAACAA, seq. 2 CCCGTATGAGTTAGAATAATA, seq. 3 AACGATGAATTACGTCGTAAA. Canine CLIP-170 target sequences; seq. a CACGCAGTTTGTGGAGTTAAA, seq. b AACTTCTATAATTGTATATAA, seq. c TAGAAAGTGTTTCACAAACAA, seq. d CAGGTGGAAGATGAAGCTAAT. Human IQGAP1 target sequences; seq. 1 CTGGGAGATAATGCCCACTTA, seq. 2 CAGGCGCTAGCTCATGAAGAA, seq 3 AATGCCATGGATGAGATTGGA (Also targets canine sequence (73). For CLIP-170-rescue experiments, 2µg of GFP-rat-CLIP-170 cDNA (58) was delivered using jetPRIME (Polyplus), according to manufacturers instructions.

CO-IP, cellular fractionation and SDS PAGE

Cell lysis and SDS PAGE was performed as described by James et al (74). For CO-IP experiments cells were lysed in M-PER Mammalian Protein Extraction Reagent (Pierce), mouse monoclonal CLIP-170 F-3 and mouse IgG (Sigma) were bound to Dynabeads protein G (Invitrogen) and Co-IP then performed as per manufacturers protocol. Rabbit polyclonal antibodies against β-actin (Abcam), α-tubulin and β-catenin were used at 1:10,000. Rabbit polyclonal antibodies against ninein (Bethyl), CLIP-170 and IQGAP1 H-103 were used at 1:2000. Mouse monoclonal antibodies against IQGAP1 and E-cadherin were used at 1:8000 and CLIP-170 F-3 at 1:2000. Secondary HRP antibodies produced in goat (Sigma) were used at 1:10,000. The membrane was analysed using a chemiluminescence detection kit (GE Healthcare). For re-probing, membranes were stripped in reblot solution (Chemicon) and antibody incubation and detection was repeated.

For cellular fractionation experiments cells were lysed in fractionation buffer (250mM sucrose, 20mM hepes pH 7.4, 10mM KCl, 1.5mM $MgCl_2$, 1mM EDTA, 1mM EGTA, 1mM DTT) for 20 mins at 0°C, the nuclear and mitochondria fractions were fractionated and discarded by consecutive centrifugation at 720G and

10,000G. The remaining supernatant containing the membrane and cytosol fractions were separated by ultracentrifugation at 100,000G for 1 hour (pellet contains membrane fraction). Each fraction was then analysed using SDS PAGE as above, with E-cadherin and α-tubulin identifying the membrane and cytosol fractions respectively.

Microscopy and statistical analysis

Cells were imaged on a Zeiss Axiovert 200M and a Zeiss LSM510 META confocal microscope. Images were processed using Axiovision (Zeiss) and Photoshop (Adobe) software.

Data for statistical analysis was first assessed for normal distribution using D'Agostino & Pearson normality test. If the data was normally distributed a parametric t-test or one-way ANOVA was applied. For data sets too small for normal distribution analysis and data not normally distributed a non-parametric Mann Whitney U-test or non-parametric Kruskal-Wallis test (with Dunn's multiple comparison post test) was used to determine significance.

MT cell-cell cortical targeting was assessed in 10μm x 10μm cortical boxes with the percentage of MTs approaching the cortex at perpendicular angles (45-90°) calculated per box and then analysed. When junctional labelling was possible, the number of cortical contacts and MT orientation was measured and analysed. MTs making cortical contact were counted for every 10μm of junction (using β-catenin staining). The imageJ (FIJI) plugin "FibrilTool" (41) was used for analysis of orientation of MTs to cell-cell junctions. This tool uses the circular average of gradients in pixel intensity across a given region of interest to find the predominant orientation and extent of alignment of "fibrillar structures". It has previously been used in quantification of the organisation of plant cortical MTs (75) and was used here to measure the general orientation of MTs relative to junctions.

For organoid analysis, the number of budding events per organoid was counted on Day 2, Day 4 and Day 6 following passaging into fresh Matrigel. This was performed in 10 regions from 3 independent experiments with >6000 organoids assessed. For each region the percentage of organoids with no buds, 1 bud, 2 buds, 3 buds and ≥4 buds was calculated.

Whole cell EB1 and centrosomal ninein intensity were measured using Volocity software (Improvision) using fixed exposure images and significance

assessed. Protein intensity analysis at cell junctions was performed using Andor iQ2 (Andor Technology). Fluorescence intensity line profiles through cell-cell junctions were measured from fixed exposure images with 21 readings taken over 2μm. The data was averaged and base-lined against background intensity. For analysis of peak intensity at cell junctions peak readings were normalised against control cells. Blind CLIP-170 comet analysis was performed in regions (10μm x 10μm boxes) on fixed exposure images with background subtraction, threshold and particle size (0.2-1.2μm^2) all applied equally to each image using ImageJ software, the number of comets per region were analysed.

GFP-CLIP-170 comet trajectories were obtained using uTrack, previously packaged as plusTipTracker (42). All post-tracking analysis was conducted using Matlab (MathWorks, 2013b) code written in-house (see supplementary information for further details). To filter out tracks that were abnormally bendy, tracks were split where the orientations of consecutive segments differed above a threshold of 30 degrees. To get better resolution at low to medium speeds (~5-15 μm/min) while comparing speeds of growth tracks between treatments, the mean speed plus one standard deviation from the “fastest” cell (which was a control cell) was taken as the maximum speed in the analysis.

Acknowledgements

The authors wish to thank Paul Wright for IT assistance and Jelena Garilovic for helpful discussions. This project was supported by the BBSRC (grant no. BB/J009040/1 to MMM and TW), the Anatomical Society and BigC Appeal (to MMM) and the Netherlands Organisation for Scientific Research (to NG).

Author contributions

D.A.G. and M.M.M. conceived and designed the experiments. D.A.G., C.R., B.J.T., J.R.G. and J.P. performed experiments and analysed data. D.A.G. assisted with figure preparations and with writing the manuscript. E.K.L. provided expertise in crypt and villus isolation. N.G. provided the knockout mice. P.T. provided expertise and assistance with microscope imaging and analyses. T.W. provided expertise in organoid generation. M.M.M. analysed data, directed the project and wrote the manuscript. All authors read and edited the manuscript.

Competing interests

The authors declare no competing financial interests.

Figure legends

Fig.1: Ninein depletion in epithelial cells

A: Scramble and ninein siRNA (seq a) depleted TC7 cells methanol fixed and stained for MTs (mAb YL1/2; green; invert) and ninein (mAb N5; red), showing loss of radial MT organisation and centrosomal focus in depleted cell. **B**: Western blot of cell lysates of scramble and ninein (seq a and 3) siRNA showing ninein (mAb Bethyl) and β-actin expression. **C:** Confocal optical sections and 3D reconstructions of scramble and ninein siRNA (seq a) depleted TC7 cells seeded for apico-basal MT array formation, fixed in methanol and labeled for MTs (mAb YL1/2) and ninein (pAb Pep3). **D**: Analysis of cell height (scramble n=284, nin siRNA seq A=251) and cross-sectional area (scramble n=190, nin siRNA seq A=200) in scramble and ninein siRNA-treated TC7 cells show decreased cell height and increased area in depleted cell (Mann-Whitney U-test $p<0.05$). Scale bars = 10μm

Fig.2: CLIP-170 and ninein in confluent and fully differentiated MDCKII cysts

A,B: Cells grown in matrigel to form 3D cysts. **A**: Optical sections of cysts fixed in methanol and stained for ninein (pAb Pep3; red) and E-cadherin (mAb, blue) showing apical localisation in (Ai) and cyst regions showing apico-basal MTs (mAb YL1/2, green in Aii; pAb alpha tubulin, red in Aiii). Optical oblique section though cyst region in Aii shows both apical and baso-lateral views with ninein (pAb N5; red) at apical cortex (arrowhead) and centrosomes (arrow) in polarised epithelial cells. Baso-lateral view of cyst epithelial cells in Aiii shows γ-tubulin (green, Aiii) at centrosomes. **B:** Optical section of cyst fixed in formaldehyde methanol and stained for CLIP-170 (pAb, green) and MTs (mAb YL1/2, red) (Bi) and cyst regions revealing apico-basal MTs (red; Bii;Biii) and apical concentration of CLIP-170 co-localising with MTs at apical cortex (Biv). **C:** Confluent cells fixed in methanol and labelled for ninein (pAb Pep3, green) and CLIP-170 (mAb F-3, red) showing some co-localisation (yellow) at cortical regions. **D**: Western blots of fractionated control and Nocodazole-treated cell lysates showing cytosol and membrane fractions, blots probed for CLIP-170 (pAb), E-cadherin (mAb) and α-tubulin (pAb). Note the double band for CLIP-170 is absent in the Nocodazole treated cell extract and this is most likely due to Nocodazole induced dephosphorylation (76). **E:** Nocodazole-treated cells expressing GFP-CLIP-170 (green) fixed in methanol and labelled for β-catenin (pAb, purple) showing cortical rings of GFP-CLIP-170. **F**: Nocodazole treated cells

fixed in methanol and stained for ninein (pAb Pep3, blue) and E-cadherin (mAb, red). Enlarged inverted junctional region showing cortical ninein remains at the cell cortex following Nocodazole treatment. Scale bars 10μm except for Aiii and Bii = 5μm.

Fig.3: Ninein and CLIP-170 in mouse small intestinal tissue and organoids

A: Isolated basal region of small intestine crypts fixed in methanol (Ai-iii) or formaldehyde methanol (Aiv,v) and stained for ninein (pAB Pep3, red)(Ai-iii), γ-tubulin (mAb, green in Ai), β-catenin (mAb, green in Aiii), CLIP-170 (pAb, green; arrow in Aiv enlarged region in Av) and MTs (mAb YL1/2, red in Aiv). Apico-basal MTs are evident in cells of the stem cell region (Aiv) but ninein is concentrated at the apical centrosome (Ai-iii) where it co-localises with γ-tubulin (inset in Ai). CLIP-170 is present as comets in cells within the stem cell region (Aiv,v). **B:** Confocal images of small intestine villus fixed in methanol (Bi-iv) or formaldehyde methanol (Bv,vi) and stained for ninein (pAb Pep3, red) and CLIP-170 (pAb, green) localised at n-MTOCs at cell apices. **Bi,iii:** Cryostat section of villus with apical ninein localisation (invert, arrow enlarged region in Biii). **Bii,iv:** Optical sections through whole mount villus showing apical views of apical surface (Bii) and junctions (Biv) (E-cadherin, mAb, green) with ninein (pAb Pep3, red) puncta at apical surface and AJ associated n-MTOCs. **Bv,vi:** Optical sections of whole mount villus stained for CLIP-170 (pAb, green) and MTs (mAb YL1/2, red) showing cross-sectional view (Bv) of CLIP-170 at apical junctional n-MTOCs and lateral view (Bvi) of villus cells with CLIP-170 concentrated at apical surface n-MTOCs (arrow) and along length of MTs. **C:** Diagram showing small intestine with crypt and villus regions and organoid generation from isolated mouse small intestinal stem cells initially leading to the formation of cell aggregates that develop into cysts and then into organoids with crypt and villus domains. **D:** MTs (mAb YL1/2, green in Di,ii and red in Diii), Ninein (pAb Pep3, red) and CLIP-170 (pAb, green) in 7 day cultured gut organoids showing apico-basal MT (mAb YL1/2) arrays in both crypt and villus-domains, with ninein concentrated at apical centrosomes (arrow in Di) in stem cell region of crypt and ninein (arrow in Dii) and CLIP-170 (arrow in Diii) at apical surface n-MTOCs in villus-domain cells. Scale bars = 5μm except for Bi =10μm.

Fig. 4: CLIP-170 siRNA knockdown in MDCKII cells leads to reduced cortical ninein and smaller cysts.

A: Western blot of lysates of control, scramble and canine CLIP-170 siRNA sequences (a-d) showing CLIP-170 and β-actin expression. **B:** Scramble and CLIP-170 siRNA-treated cells fixed in methanol and stained for ninein (pAb N5, blue and invert) and CLIP-170 (mAb, red). **C**: Junction fluorescence intensity profile analyses (n=128) of ninein in scramble and CLIP-170-depleted cells. **D**: Relative peak intensities of ninein at junctions in scramble and CLIP-170 siRNA-depleted cells reveal a significant decrease in ninein intensity in depleted cells (Mann Whitney U-test $p<0.05$). **E**: Western blot of lysates of control, scramble, CLIP-170 siRNA, IQGAP1 siRNA and Rac1 inhibitor NSC23766 (250μM) treatments showing ninein (pAb Bethyl) and β-actin (pAb) expression. **F:** Relative centrosomal ninein fluorescence intensity (n=50) in control, scramble, CLIP-170 siRNA and Rac1 inhibitor NSC23766 (250μM) treated cells revealing no significant difference (unpaired t-test). **G:** Scramble and CLIP-170 siRNA treated cells grown in Matrigel to induce cyst formation and fixed in formaldehyde methanol and stained for MTs (mAb YL1/2, red) and CLIP-170 (pAb, green) at day 6 showing apico-basal MTs in both scramble and knockdown cysts. Note the marked decrease in cysts size in CLIP-170 siRNA treated cysts. Inset shows MTs in depleted cell (arrow). **H:** Cyst sizes in scramble and CLIP-170 depleted cells based on cross-sectional areas in μm^2 with bars indicating averages showing significantly smaller cyst area in knockdown (Mann Whitney U-test $p<0.05$). Scale bars: 10μm.

Fig. 5: Small intestine of the *Clip1/Clip2* double knockout mouse.

A: Confocal optical sections of small intestinal crypts of WT and *Clip1/Clip2* KO mice fixed in formaldehyde methanol and stained for CLIP-170 (pAb, invert) showing loss of CLIP-170 staining in knockout crypt. **B:** Confocal images showing lateral views of paraformaldehyde fixed villus cells labeled for gp135 (rat mAb, green) and stained for DNA with DAPI (red) indicating markedly less apical gp135 in the KO compared with WT. **C:** Optical sections at the level of the apical centrosome in WT and KO villus cells fixed in formaldehyde methanol and labeled for acetylated tubulin (mAb) showing centrioles in KO cells but no evidence of centrioles in WT (arrows). The arrowed regions are enlarged in inset below. **D:** Phase contrast images showing different stages of organoid (WT) development

from cyst formation with no buds to fully formed organoids with several crypts (buds). **E:** Graph showing the percentage of organoids with 0, 1, 2, 3 or more than 4 buds at day 2, 4 and 6 of development in organoids generated from WT and KO small intestine. Note that the formation of crypts (buds) is much slower in the KO compared to WT. Scale bars: A,C=10μm, B=5μm D=20μm. 2 way Anova statistical testing WT vs KO, Day 2, Day 4, Day 6 $p<0.05$.

Fig.6: Loss of ninein at n-MTOCs in *Clip1/Clip2* double knockout mouse intestine.

A: Confocal images of methanol fixed villus cells stained for ninein (pAb Pep3, red) and β-catenin (mAb, green) showing baso-lateral and apical cross-sectional views and revealing almost total absence of ninein at apical surface n-MTOCs in KO. **B:** Fluorescence intensity profiles for β-catenin (n=112) and ninein (n=112) at junctions in WT and KO villus. **C**: Relative peak fluorescence intensities for β-catenin and ninein at junctional sites in WT and KO villus revealing no significant difference in junctional β-catenin but a significant reduction in ninein (Mann Whitney U-test). **D:** Confocal sections showing baso-lateral views of methanol fixed villus cells stained for γ-tubulin (mAb, green) and β-catenin (pAb, red) revealing γ-tubulin at apical n-MTOCs in both WT and KO. Scale bars = 5μm.

Fig.7: CLIP-170 siRNA depletion leads to compromised MT cortical targeting

A: ARPE-19 cell methanol fixed and labelled for MTs (mAb YL1/2, purple) and CLIP-170 (pAb, green; enlarged region arrowed). **B:** Western blot of lysates from control, scramble and CLIP-170 siRNA (human seq 1 and 2) ARPE-19 cells showing CLIP-170 (pAb) and β-actin expression. **C**: Mixed culture showing a scramble cell next to a CLIP-170 siRNA-depleted cell (*) stained for CLIP-170 (pAb, green, invert) and MTs (mAb YL1/2, purple, invert). **D**: Cell-cell contact between a scramble (top) and CLIP-170-depleted (bottom) cell with perpendicular cortical targeting MTs highlighted in red and MTs parallel to the cell cortex in blue. **E:** Graph showing mean (n=30) percentage of MTs with perpendicular approach to cell-cell contacts in control, scramble, CLIP-170 siRNA, GFP-CLIP-170 rescue and IQGAP1 siRNA-treated cells. A non-parametric one-way ANOVA with Dunn's multiple comparison post test was used and revealed no significance between control and scramble and between scramble and CLIP-170 rescue but significant differences

between scramble and CLIP-170 siRNA, between Scramble and IQGAP1 siRNA and between CLIP-170 siRNA and CLIP-170 rescue. **F:** GFP-CLIP-170 (green, invert) expressing ARPE-19 cell (arrow) next to a CLIP-170-depleted cell, showing rescue of radial MT (purple, invert) organisation. **G:** Mixed culture of scramble and CLIP-170 siRNA (*) cells fixed 30 minutes following Nocodazole removal and stained for MTs (purple, invert) and CLIP-170 green). The enlarged region of cell-cell contact (dotted red line) between scramble (right) and CLIP-170-depleted (left) cells shows lack of perpendicular MT approach in depleted cell. GFP-CLIP-170 (green) expressing ARPE-19 cell next to a CLIP-170 depleted cell (*) showing rescue of radial MT (purple) organisation 30 mins after Nocodazole removal. **H**: Graph showing mean (n=30) percentage of MTs with perpendicular approach to cell-cell contacts following Nocodazole washout in control, scramble and CLIP-170 siRNA cells showing no significance between control and scramble but significant differences between control and CLIP-170 siRNA and between scramble and CLIP-170 siRNA (Mann Whitney U-test). Scale bars: 5μm. Except for A=10μm

Fig.8: IQGAP1 siRNA depletion leads to loss of MT cortical targeting and reduced ninein at n-MTOCs

A: Western blot of Co-IP experiments using either CLIP-170 or IgG as bait to pulldown protein complexes in TC7 cells showing CLIP-170 pulls down endogenous CLIP-170, IQGAP1 and β-catenin but not the IgG control lanes (CLIP-170 pAb was used for probing but mAb used as bait). **B:** ARPE-19 cells methanol fixed and stained for IQGAP1 (mAb), MTs (YL1/2) and β-catenin (pAb) purple in Bi indicating co-localisation and Nocodazole recovery (Bii) showing CLIP-170 bound MTs targeting cortical IQGAP1 located on the inner face of junctional β-catenin puncta. Arrow indicates region enlarged in inset to the left. **C**: Mixed culture of ARPE-19 cells fixed in methanol showing a scramble cell next to a IQGAP1 depleted cell (*) stained for IQGAP1 (mAb, red, invert) and MTs (rab alpha tubulin, blue, invert). Enlarged region (arrow) showing lack of cortical MT targeting in IQGAP1 depleted cell. **D:** Western blots of lysates of control, scramble and IQGAP1 siRNA ARPE-19 and cells showing IQGAP1 and β-actin expression. **E:** Scramble and IQGAP1 siRNA treated cells methanol fixed and stained for ninein (pAb Pep3, green) and IQGAP1 (mAb, red) showing less cortical ninein in depleted cells. **F:** Junctional fluorescence intensity profile (n=92) for ninein in scramble and IQGAP1 siRNA-

treated cells. **G:** Relative peak fluorescence intensities for β-catenin and ninein at junctions in scramble and IQGAP1 siRNA-treated cells showing no significance in β-catenin intensities (unpaired t-test) but a significant reduction in ninein (non=parametric Mann Whitney $p<0.05$). Scale bars = 10μm except Bii = 2μm.

Fig.9: Rac1 inhibition leads to reduced cortical ninein and MT junctional targeting

A: Control and Rac1-inhibited (250 μM NSC23766) cells methanol fixed and stained for ninein (pAb N5, green, invert) and β-catenin (mAb, red, invert) showing a marked reduction in cortical ninein in Rac1 inhibited cells. **B:** Junctional fluorescence intensity profile for ninein (n=112) in control and Rac1-inhibited cells. **C:** Relative peak fluorescence intensity of E-cadherin and ninein at junctions in control and Rac1-inhibited cells showing no significance in E-cadherin but in ninein (non-parametric Mann Whitney $p<0.05$). **D:** Control and Rac1-inhibited (250μM NSC23766) ARPE-19 cells methanol fixed and stained for β-catenin (mAb, purple) and MTs (pAb alpha tubulin, green), with enlarged regions (arrowed) highlighting cortical MT approaches. Note several MTs aligned parallel to the cortex in Rac1 inhibited cells. **E**: Graph showing mean MT orientation to cell junctions (n=30), using FibrilTool (41) revealing significant deviation from perpendicular targeting in inhibited cells (non-parametric Mann Whitney ***). **F**: Graph showing the mean (n=30) number of MT contacts per 10μm junctional β-catenin staining revealing significantly fewer cortical contacts in inhibited cells (unpaired t-test $p<0.05$). Scale bars 10μm.

Fig.10 Rac1 inhibition leads to fewer and slower CLIP-170 comets and decreased pausing events

A: Control and Rac1-inhibited (250μM NSC23766) ARPE-19 cells fixed in formaldehyde methanol and stained for CLIP-170 (pAb) and MTs (mAb YL1/2) with enlargements of comets. **B**: Graph showing the mean number of CLIP-170 comets (n=30) for each treatment showing a reduction in comets with Rac1 inhibition. **C-G**: GFP-CLIP-170 dynamics in control and Rac1-inhibited ARPE-19 cells. **C-D**: Mean (n=4) percentage of composite tracks defined as growing or pausing. Only top part of graph is shown in C. **E-F**: Analysis of mean (n=4) GFP- CLIP-170 comet speed and growth length. **G:** Plots of GFP-CLIP-170 growth tracks colour coded according

to speed with bar plot showing mean (n=4) percentage of tracks in each speed group. See also movies 1 and 2. Scale bars: 10μm. **B-F** non-parametric Mann Whitney $p<0.05$.

Fig.11: Apico-basal MTs and CAMSAP2 and p150^{Glued} at n-MTOCs in both WT and KO villus cells

A: Formaldehyde methanol fixed isolated villus epithelial tissue (right) stained for MTs (mAb YL1/2) and organoid villus-domain epithelial cells (left) stained for MTs (blue) and β-catenin (pAb, red) showing apico-basal MTs in both WT and KO. **B**: Villus stained for p150^{Glued} (mAb, green) and β-catenin (pAb, red) showing apical surface and junction localisation in both WT and KO. **C:** Isolated WT villus tissue labeled for p150^{Glued} (mAb, green) and MTs (pAb alpha tubulin, red) showing apical concentration of 150^{Glued} at n-MTOCs and apico-basal MTs with minus-ends targeting p150^{Glued} puncta (arrow indicated enlarged area to left). **D:** Organoid villus-domain cells stained for CAMSAP2 (pAb, purple) and β-catenin (mAb, green) showing CAMSAP2 puncta at apical surface n-MTOCs in organoids generated from both WT and KO small intestine. Scale bars: 5μm.

Fig.12: Models for ninein redeployment to n-MTOCs during epithelial differentiation

Model 1: A: CLIP-170 (green) bound MTs elongate and target IQGAP1 (blue) at adherens junctions (yellow) in a process promoted by active Rac1 (pink). **B:** CLIP-170, IQGAP1 and active Rac1 facilitate MT capture at adherens junction associated n-MTOCs and ninein (red) is transported along MTs. **C:** Ninein and CLIP-170 bind to adherens junctions, MT minus-ends are released from centrosome and plus-ends elongate towards the cell base. **D:** Ninein anchors MT minus-ends at n-MTOCs at adherens junctions while plus-ends elongate towards cell base thus generating the apico-basal array.

Model 2: A: CLIP-170 (green) is recruited to apical adherens junctions (yellow) and forms a complex with IQGAP1 (blue) and active Rac1 (pink). **B:** Cortical receptor complex IQGAP1, CLIP-170 and active Rac1 recruits ninein (red) to apical adherens junctions. **C:** Ninein accumulates at forming n-MTOCs associated with apical adherens junctions. **D:** MT (black) minus-ends are captured by ninein at n-MTOCs and plus-ends elongated towards cell base.

References

1. Bacallao R, Antony C, Dotti C, Karsenti E, Stelzer EH, Simons K. The subcellular organization of Madin-Darby canine kidney cells during the formation of a polarized epithelium. The Journal of cell biology. 1989 Dec;109(6 Pt 1):2817-32. PubMed PMID: 2592406. Pubmed Central PMCID: 2115929.
2. Meads T, Schroer TA. Polarity and nucleation of microtubules in polarized epithelial cells. Cell motility and the cytoskeleton. 1995;32(4):273-88. PubMed PMID: 8608606.
3. Mogensen MM, Tucker JB, Stebbings H. Microtubule polarities indicate that nucleation and capture of microtubules occurs at cell surfaces in Drosophila. The Journal of cell biology. 1989 Apr;108(4):1445-52. PubMed PMID: 2925791. Pubmed Central PMCID: 2115526.
4. Sanchez AD, Feldman JL. Microtubule-organizing centers: from the centrosome to non-centrosomal sites. Current opinion in cell biology. 2016 Sep 22. PubMed PMID: 27666167.
5. Mogensen MM, Tucker JB, Mackie JB, Prescott AR, Nathke IS. The adenomatous polyposis coli protein unambiguously localizes to microtubule plus ends and is involved in establishing parallel arrays of microtubule bundles in highly polarized epithelial cells. The Journal of cell biology. 2002 Jun 10;157(6):1041-8. PubMed PMID: 12058019. Pubmed Central PMCID: 2174057.
6. Bellett G, Carter JM, Keynton J, Goldspink D, James C, Moss DK, et al. Microtubule plus-end and minus-end capture at adherens junctions is involved in the assembly of apico-basal arrays in polarised epithelial cells. Cell motility and the cytoskeleton. 2009 Oct;66(10):893-908. PubMed PMID: 19479825.
7. Mogensen MM, Malik A, Piel M, Bouckson-Castaing V, Bornens M. Microtubule minus-end anchorage at centrosomal and non-centrosomal sites: the role of ninein. Journal of cell science. 2000 Sep;113 (Pt 17):3013-23. PubMed PMID: 10934040.
8. Moss DK, Bellett G, Carter JM, Liovic M, Keynton J, Prescott AR, et al. Ninein is released from the centrosome and moves bi-directionally along microtubules. Journal of cell science. 2007 Sep 1;120(Pt 17):3064-74. PubMed PMID: 17698918.
9. Gierke S, Wittmann T. EB1-recruited microtubule +TIP complexes coordinate protrusion dynamics during 3D epithelial remodeling. Current biology : CB. 2012 May 8;22(9):753-62. PubMed PMID: 22483942. Pubmed Central PMCID: 3350573.
10. Wittmann T, Bokoch GM, Waterman-Storer CM. Regulation of microtubule destabilizing activity of Op18/stathmin downstream of Rac1. The Journal of biological chemistry. 2004 Feb 13;279(7):6196-203. PubMed PMID: 14645234.
11. Ameen NA, Figueroa Y, Salas PJ. Anomalous apical plasma membrane phenotype in CK8-deficient mice indicates a novel role for intermediate filaments in the polarization of simple epithelia. Journal of cell science. 2001 Feb;114(Pt 3):563-75. PubMed PMID: 11171325.
12. Feldman JL, Priess JR. A role for the centrosome and PAR-3 in the hand-off of MTOC function during epithelial polarization. Current biology : CB. 2012 Apr 10;22(7):575-82. PubMed PMID: 22425160. Pubmed Central PMCID: 3409831.

13. Dauber A, Lafranchi SH, Maliga Z, Lui JC, Moon JE, McDeed C, et al. Novel microcephalic primordial dwarfism disorder associated with variants in the centrosomal protein ninein. The Journal of clinical endocrinology and metabolism. 2012 Nov;97(11):E2140-51. PubMed PMID: 22933543. Pubmed Central PMCID: 3485598.
14. Grosch M, Gruner B, Spranger S, Stutz AM, Rausch T, Korbel JO, et al. Identification of a Ninein (NIN) mutation in a family with spondyloepimetaphyseal dysplasia with joint laxity (leptodactylic type)-like phenotype. Matrix biology : journal of the International Society for Matrix Biology. 2013 Oct-Nov;32(7-8):387-92. PubMed PMID: 23665482.
15. Matsumoto T, Schiller P, Dieterich LC, Bahram F, Iribe Y, Hellman U, et al. Ninein is expressed in the cytoplasm of angiogenic tip-cells and regulates tubular morphogenesis of endothelial cells. Arteriosclerosis, thrombosis, and vascular biology. 2008 Dec;28(12):2123-30. PubMed PMID: 18772498.
16. Ohama Y, Hayashi K. Relocalization of a microtubule-anchoring protein, ninein, from the centrosome to dendrites during differentiation of mouse neurons. Histochemistry and cell biology. 2009 Nov;132(5):515-24. PubMed PMID: 19690882.
17. Wang X, Tsai JW, Imai JH, Lian WN, Vallee RB, Shi SH. Asymmetric centrosome inheritance maintains neural progenitors in the neocortex. Nature. 2009 Oct 15;461(7266):947-55. PubMed PMID: 19829375. Pubmed Central PMCID: 2764320.
18. Abal M, Piel M, Bouckson-Castaing V, Mogensen M, Sibarita JB, Bornens M. Microtubule release from the centrosome in migrating cells. The Journal of cell biology. 2002 Dec 9;159(5):731-7. PubMed PMID: 12473683. Pubmed Central PMCID: 2173398.
19. Dammermann A, Merdes A. Assembly of centrosomal proteins and microtubule organization depends on PCM-1. The Journal of cell biology. 2002 Oct 28;159(2):255-66. PubMed PMID: 12403812. Pubmed Central PMCID: 2173044.
20. Delgehyr N, Sillibourne J, Bornens M. Microtubule nucleation and anchoring at the centrosome are independent processes linked by ninein function. Journal of cell science. 2005 Apr 15;118(Pt 8):1565-75. PubMed PMID: 15784680.
21. Lechler T, Fuchs E. Desmoplakin: an unexpected regulator of microtubule organization in the epidermis. The Journal of cell biology. 2007 Jan 15;176(2):147-54. PubMed PMID: 17227889. Pubmed Central PMCID: 2063934.
22. Goldspink DA, Gadsby JR, Bellett G, Keynton J, Tyrrell BJ, Lund EK, et al. The microtubule end-binding protein EB2 is a central regulator of microtubule reorganisation in apico-basal epithelial differentiation. Journal of cell science. 2013 Sep 1;126(Pt 17):4000-14. PubMed PMID: 23813963.
23. Straube A, Merdes A. EB3 regulates microtubule dynamics at the cell cortex and is required for myoblast elongation and fusion. Current biology : CB. 2007 Aug 7;17(15):1318-25. PubMed PMID: 17658256. Pubmed Central PMCID: 1971230.
24. Zhang T, Zaal KJ, Sheridan J, Mehta A, Gundersen GG, Ralston E. Microtubule plus-end binding protein EB1 is necessary for muscle cell differentiation, elongation and fusion. Journal of cell science. 2009 May 1;122(Pt 9):1401-9. PubMed PMID: 19366726. Pubmed Central PMCID: 2671926.

25. Perez F, Diamantopoulos GS, Stalder R, Kreis TE. CLIP-170 highlights growing microtubule ends in vivo. Cell. 1999 Feb 19;96(4):517-27. PubMed PMID: 10052454.
26. Komarova YA, Akhmanova AS, Kojima S, Galjart N, Borisy GG. Cytoplasmic linker proteins promote microtubule rescue in vivo. The Journal of cell biology. 2002 Nov 25;159(4):589-99. PubMed PMID: 12446741. Pubmed Central PMCID: 2173097.
27. Galjart N. Plus-end-tracking proteins and their interactions at microtubule ends. Current biology : CB. 2010 Jun 22;20(12):R528-37. PubMed PMID: 20620909.
28. Ligon LA, Holzbaur EL. Microtubules tethered at epithelial cell junctions by dynein facilitate efficient junction assembly. Traffic. 2007 Jul;8(7):808-19. PubMed PMID: 17550375.
29. Shaw RM, Fay AJ, Puthenveedu MA, von Zastrow M, Jan YN, Jan LY. Microtubule plus-end-tracking proteins target gap junctions directly from the cell interior to adherens junctions. Cell. 2007 Feb 9;128(3):547-60. PubMed PMID: 17289573. Pubmed Central PMCID: 1955433.
30. Stehbens SJ, Paterson AD, Crampton MS, Shewan AM, Ferguson C, Akhmanova A, et al. Dynamic microtubules regulate the local concentration of E-cadherin at cell-cell contacts. Journal of cell science. 2006 May 1;119(Pt 9):1801-11. PubMed PMID: 16608875.
31. Fukata M, Watanabe T, Noritake J, Nakagawa M, Yamaga M, Kuroda S, et al. Rac1 and Cdc42 capture microtubules through IQGAP1 and CLIP-170. Cell. 2002 Jun 28;109(7):873-85. PubMed PMID: 12110184.
32. Wacker IU, Rickard JE, De Mey JR, Kreis TE. Accumulation of a microtubule-binding protein, pp170, at desmosomal plaques. The Journal of cell biology. 1992 May;117(4):813-24. PubMed PMID: 1349608. Pubmed Central PMCID: 2289468.
33. Larance M, Ahmad Y, Kirkwood KJ, Ly T, Lamond AI. Global subcellular characterization of protein degradation using quantitative proteomics. Molecular & cellular proteomics : MCP. 2013 Mar;12(3):638-50. PubMed PMID: 23242552. Pubmed Central PMCID: 3591657.
34. van der Flier LG, Clevers H. Stem cells, self-renewal, and differentiation in the intestinal epithelium. Annual review of physiology. 2009;71:241-60. PubMed PMID: 18808327.
35. Komarova Iu A, Vorob'ev IA. [The ultrastructure of the cell center in the enterocytes of mouse embryos and newborn mice]. Ontogenez. 1994 Mar-Apr;25(2):76-88. PubMed PMID: 8190453. Ul'trastruktura kletochnogo tsentra v enterotsitakh u embrionov i novorozhdennykh myshei.
36. Sato T, Vries RG, Snippert HJ, van de Wetering M, Barker N, Stange DE, et al. Single Lgr5 stem cells build crypt-villus structures in vitro without a mesenchymal niche. Nature. 2009 May 14;459(7244):262-5. PubMed PMID: 19329995.
37. Fukata M, Kuroda S, Nakagawa M, Kawajiri A, Itoh N, Shoji I, et al. Cdc42 and Rac1 regulate the interaction of IQGAP1 with beta-catenin. The Journal of biological chemistry. 1999 Sep 10;274(37):26044-50. PubMed PMID: 10473551.
38. Noritake J, Watanabe T, Sato K, Wang S, Kaibuchi K. IQGAP1: a key regulator of adhesion and migration. Journal of cell science. 2005 May 15;118(Pt 10):2085-92. PubMed PMID: 15890984.

39. Waterman-Storer CM, Worthylake RA, Liu BP, Burridge K, Salmon ED. Microtubule growth activates Rac1 to promote lamellipodial protrusion in fibroblasts. Nature cell biology. 1999 May;1(1):45-50. PubMed PMID: 10559863.
40. Gao Y, Dickerson JB, Guo F, Zheng J, Zheng Y. Rational design and characterization of a Rac GTPase-specific small molecule inhibitor. Proceedings of the National Academy of Sciences of the United States of America. 2004 May 18;101(20):7618-23. PubMed PMID: 15128949. Pubmed Central PMCID: 419655.
41. Boudaoud A, Burian A, Borowska-Wykret D, Uyttewaal M, Wrzalik R, Kwiatkowska D, et al. FibrilTool, an ImageJ plug-in to quantify fibrillar structures in raw microscopy images. Nature protocols. 2014 Feb;9(2):457-63. PubMed PMID: 24481272.
42. Applegate KT, Besson S, Matov A, Bagonis MH, Jaqaman K, Danuser G. plusTipTracker: Quantitative image analysis software for the measurement of microtubule dynamics. Journal of structural biology. 2011 Nov;176(2):168-84. PubMed PMID: 21821130. Pubmed Central PMCID: 3298692.
43. Quintyne NJ, Gill SR, Eckley DM, Crego CL, Compton DA, Schroer TA. Dynactin is required for microtubule anchoring at centrosomes. The Journal of cell biology. 1999 Oct 18;147(2):321-34. PubMed PMID: 10525538. Pubmed Central PMCID: 2174233.
44. Goodwin SS, Vale RD. Patronin regulates the microtubule network by protecting microtubule minus ends. Cell. 2010 Oct 15;143(2):263-74. PubMed PMID: 20946984. Pubmed Central PMCID: 3008421.
45. Meng W, Mushika Y, Ichii T, Takeichi M. Anchorage of microtubule minus ends to adherens junctions regulates epithelial cell-cell contacts. Cell. 2008 Nov 28;135(5):948-59. PubMed PMID: 19041755.
46. Zheng J, Furness D, Duan C, Miller KK, Edge RM, Chen J, et al. Marshalin, a microtubule minus-end binding protein, regulates cytoskeletal structure in the organ of Corti. Biology open. 2013;2(11):1192-202. PubMed PMID: 24244856. Pubmed Central PMCID: 3828766.
47. Jiang K, Hua S, Mohan R, Grigoriev I, Yau KW, Liu Q, et al. Microtubule minus-end stabilization by polymerization-driven CAMSAP deposition. Developmental cell. 2014 Feb 10;28(3):295-309. PubMed PMID: 24486153.
48. Bartolini F, Gundersen GG. Generation of noncentrosomal microtubule arrays. Journal of cell science. 2006 Oct 15;119(Pt 20):4155-63. PubMed PMID: 17038542.
49. Mogensen MM. Microtubule release and capture in epithelial cells. Biology of the cell / under the auspices of the European Cell Biology Organization. 1999 May-Jun;91(4-5):331-41. PubMed PMID: 10518999.
50. Wang S, Wu D, Quintin S, Green RA, Cheerambathur DK, Ochoa SD, et al. NOCA-1 functions with gamma-tubulin and in parallel to Patronin to assemble non-centrosomal microtubule arrays in C. elegans. eLife. 2015;4. PubMed PMID: 26371552. Pubmed Central PMCID: 4608005.
51. Fukata M, Nakagawa M, Itoh N, Kawajiri A, Yamaga M, Kuroda S, et al. Involvement of IQGAP1, an effector of Rac1 and Cdc42 GTPases, in cell-cell dissociation during cell scattering. Molecular and cellular biology. 2001 Mar;21(6):2165-83. PubMed PMID: 11238950. Pubmed Central PMCID: 86844.
52. Kuroda S, Fukata M, Nakagawa M, Fujii K, Nakamura T, Ookubo T, et al. Role of IQGAP1, a target of the small GTPases Cdc42 and Rac1, in regulation of E-

cadherin- mediated cell-cell adhesion. Science. 1998 Aug 7;281(5378):832-5. PubMed PMID: 9694656.
53. Grigoriev I, Borisy G, Vorobjev I. Regulation of microtubule dynamics in 3T3 fibroblasts by Rho family GTPases. Cell motility and the cytoskeleton. 2006 Jan;63(1):29-40. PubMed PMID: 16362953.
54. Tian Y, Tian X, Gawlak G, O'Donnell JJ, 3rd, Sacks DB, Birukova AA. IQGAP1 regulates endothelial barrier function via EB1-cortactin cross talk. Molecular and cellular biology. 2014 Sep 15;34(18):3546-58. PubMed PMID: 25022754. Pubmed Central PMCID: 4135611.
55. Kodani A, Salome Sirerol-Piquer M, Seol A, Garcia-Verdugo JM, Reiter JF. Kif3a interacts with Dynactin subunit p150 Glued to organize centriole subdistal appendages. The EMBO journal. 2013 Feb 20;32(4):597-607. PubMed PMID: 23386061. Pubmed Central PMCID: 3579144.
56. Gavilan MP, Arjona M, Zurbano A, Formstecher E, Martinez-Morales JR, Bornens M, et al. Alpha-catenin-dependent recruitment of the centrosomal protein CAP350 to adherens junctions allows epithelial cells to acquire a columnar shape. PLoS biology. 2015 Mar;13(3):e1002087. PubMed PMID: 25764135. Pubmed Central PMCID: 4357431.
57. Hoppeler-Lebel A, Celati C, Bellett G, Mogensen MM, Klein-Hitpass L, Bornens M, et al. Centrosomal CAP350 protein stabilises microtubules associated with the Golgi complex. Journal of cell science. 2007 Sep 15;120(Pt 18):3299-308. PubMed PMID: 17878239.
58. Akhmanova A, Mausset-Bonnefont AL, van Cappellen W, Keijzer N, Hoogenraad CC, Stepanova T, et al. The microtubule plus-end-tracking protein CLIP-170 associates with the spermatid manchette and is essential for spermatogenesis. Genes & development. 2005 Oct 15;19(20):2501-15. PubMed PMID: 16230537. Pubmed Central PMCID: 1257404.
59. Binker MG, Zhao DY, Pang SJ, Harrison RE. Cytoplasmic linker protein-170 enhances spreading and phagocytosis in activated macrophages by stabilizing microtubules. Journal of immunology. 2007 Sep 15;179(6):3780-91. PubMed PMID: 17785815.
60. Galjart N. CLIPs and CLASPs and cellular dynamics. Nature reviews Molecular cell biology. 2005 Jun;6(6):487-98. PubMed PMID: 15928712.
61. Stoops EH, Hull M, Olesen C, Mistry K, Harder JL, Rivera-Molina F, et al. The periciliary ring in polarized epithelial cells is a hot spot for delivery of the apical protein gp135. The Journal of cell biology. 2015 Oct 26;211(2):287-94. PubMed PMID: 26504168. Pubmed Central PMCID: 4621837.
62. Mrozowska PS, Fukuda M. Regulation of podocalyxin trafficking by Rab small GTPases in 2D and 3D epithelial cell cultures. The Journal of cell biology. 2016 May 2. PubMed PMID: 27138252.
63. Sumigray KD, Lechler T. Desmoplakin controls microvilli length but not cell adhesion or keratin organization in the intestinal epithelium. Molecular biology of the cell. 2012 Mar;23(5):792-9. PubMed PMID: 22238362. Pubmed Central PMCID: 3290639.
64. Tanaka N, Meng W, Nagae S, Takeichi M. Nezha/CAMSAP3 and CAMSAP2 cooperate in epithelial-specific organization of noncentrosomal microtubules. Proceedings of the National Academy of Sciences of the United States of America. 2012 Dec 4;109(49):20029-34. PubMed PMID: 23169647. Pubmed Central PMCID: 3523837.

65. Yau KW, van Beuningen SF, Cunha-Ferreira I, Cloin BM, van Battum EY, Will L, et al. Microtubule minus-end binding protein CAMSAP2 controls axon specification and dendrite development. Neuron. 2014 Jun 4;82(5):1058-73. PubMed PMID: 24908486.
66. Toya M, Kobayashi S, Kawasaki M, Shioi G, Kaneko M, Ishiuchi T, et al. CAMSAP3 orients the apical-to-basal polarity of microtubule arrays in epithelial cells. Proceedings of the National Academy of Sciences of the United States of America. 2015 Dec 29. PubMed PMID: 26715742.
67. Noordstra I, Liu Q, Nijenhuis W, Hua S, Jiang K, Baars M, et al. Control of apico-basal epithelial polarity by the microtubule minus-end-binding protein CAMSAP3 and spectraplakin ACF7. Journal of cell science. 2016 Nov 15;129(22):4278-88. PubMed PMID: 27802168.
68. Khanal I, Elbediwy A, Diaz de la Loza Mdel C, Fletcher GC, Thompson BJ. Shot and Patronin polarise microtubules to direct membrane traffic and biogenesis of microvilli in epithelia. Journal of cell science. 2016 Jul 1;129(13):2651-9. PubMed PMID: 27231092. Pubmed Central PMCID: 4958304.
69. Hoogenraad CC, Koekkoek B, Akhmanova A, Krugers H, Dortland B, Miedema M, et al. Targeted mutation of Cyln2 in the Williams syndrome critical region links CLIP-115 haploinsufficiency to neurodevelopmental abnormalities in mice. Nature genetics. 2002 Sep;32(1):116-27. PubMed PMID: 12195424.
70. Belshaw NJ, Pal N, Tapp HS, Dainty JR, Lewis MP, Williams MR, et al. Patterns of DNA methylation in individual colonic crypts reveal aging and cancer-related field defects in the morphologically normal mucosa. Carcinogenesis. 2010 Jun;31(6):1158-63. PubMed PMID: 20395289.
71. Whitehead RH, VanEeden PE, Noble MD, Ataliotis P, Jat PS. Establishment of conditionally immortalized epithelial cell lines from both colon and small intestine of adult H-2Kb-tsA58 transgenic mice. Proceedings of the National Academy of Sciences of the United States of America. 1993 Jan 15;90(2):587-91. PubMed PMID: 7678459. Pubmed Central PMCID: 45708.
72. Coquelle FM, Caspi M, Cordelieres FP, Dompierre JP, Dujardin DL, Koifman C, et al. LIS1, CLIP-170's key to the dynein/dynactin pathway. Molecular and cellular biology. 2002 May;22(9):3089-102. PubMed PMID: 11940666. Pubmed Central PMCID: 133759.
73. Noritake J, Fukata M, Sato K, Nakagawa M, Watanabe T, Izumi N, et al. Positive role of IQGAP1, an effector of Rac1, in actin-meshwork formation at sites of cell-cell contact. Molecular biology of the cell. 2004 Mar;15(3):1065-76. PubMed PMID: 14699063. Pubmed Central PMCID: 363077.
74. James C, Collison DJ, Duncan G. Characterization and functional activity of thrombin receptors in the human lens. Investigative ophthalmology & visual science. 2005 Mar;46(3):925-32. PubMed PMID: 15728549.
75. Uyttewaal M, Burian A, Alim K, Landrein B, Borowska-Wykret D, Dedieu A, et al. Mechanical stress acts via katanin to amplify differences in growth rate between adjacent cells in Arabidopsis. Cell. 2012 Apr 13;149(2):439-51. PubMed PMID: 22500806.
76. Rickard JE, Kreis TE. Binding of pp170 to microtubules is regulated by phosphorylation. The Journal of biological chemistry. 1991 Sep 15;266(26):17597-605. PubMed PMID: 1680130.

Fig.1. **Ninein depletion in epithelial cells**

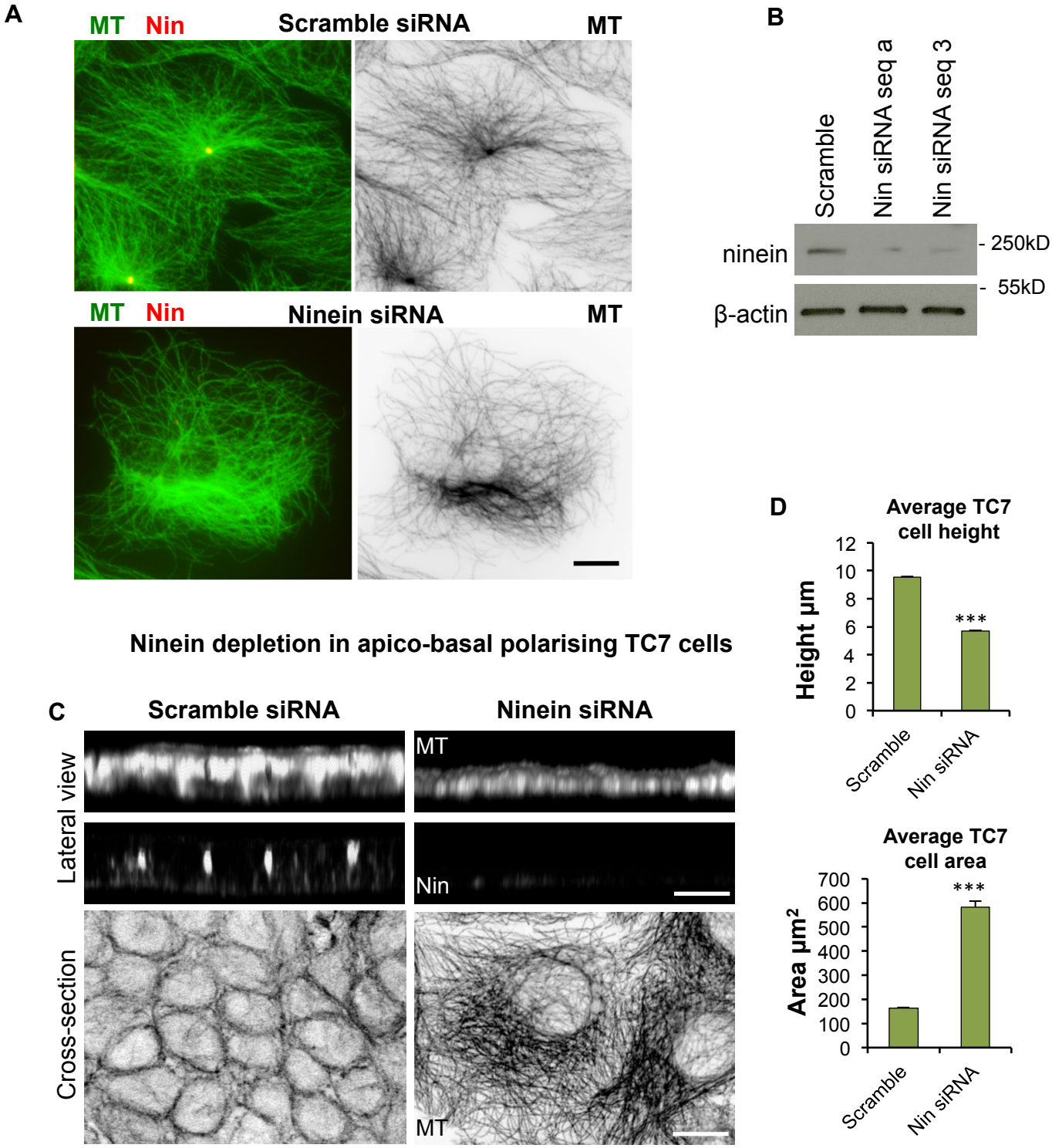

Fig.2. CLIP-170 and ninein in polarised 3D MDCKII cysts

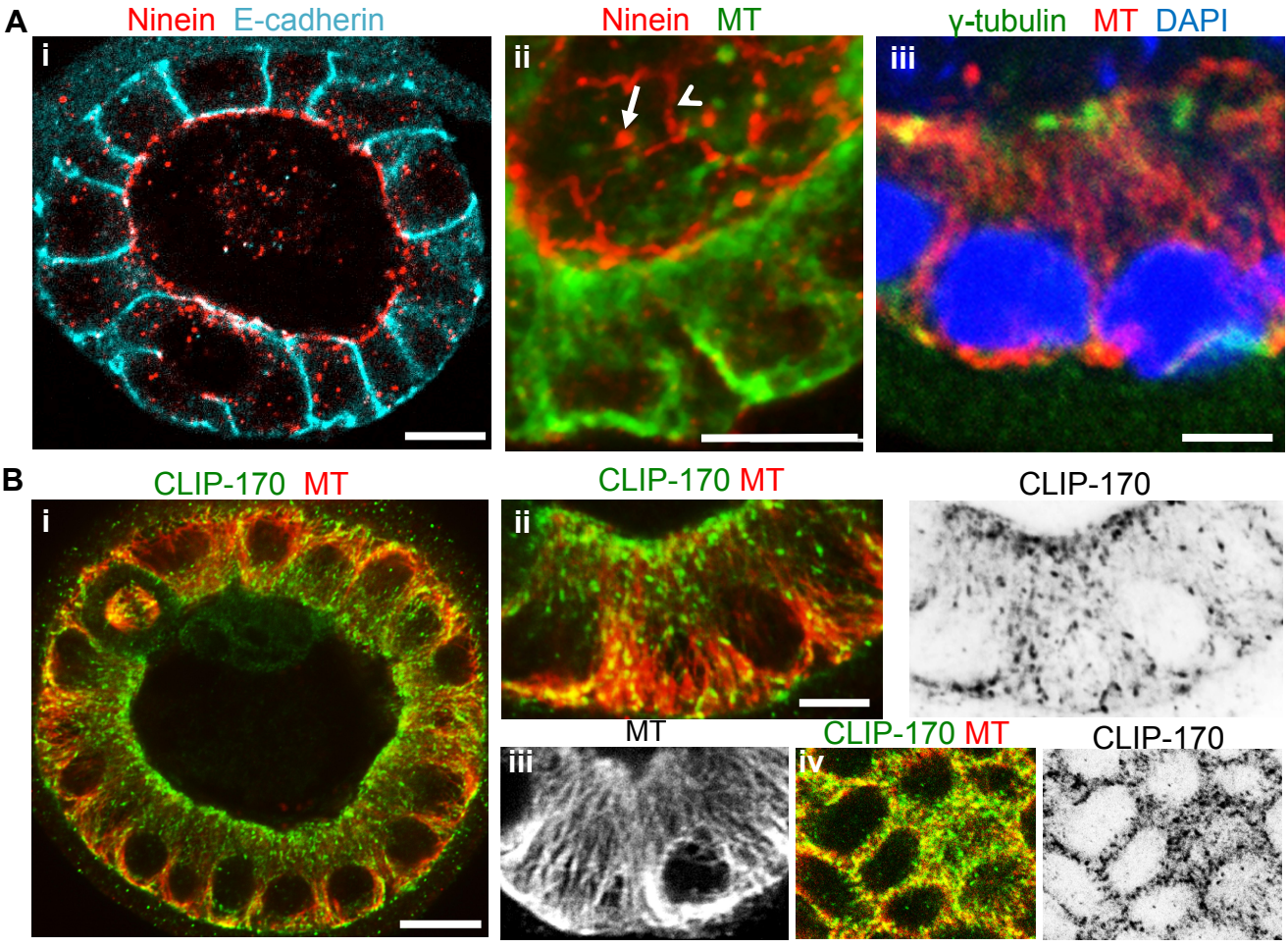

CLIP-170 and Ninein membrane localisation and fractionation

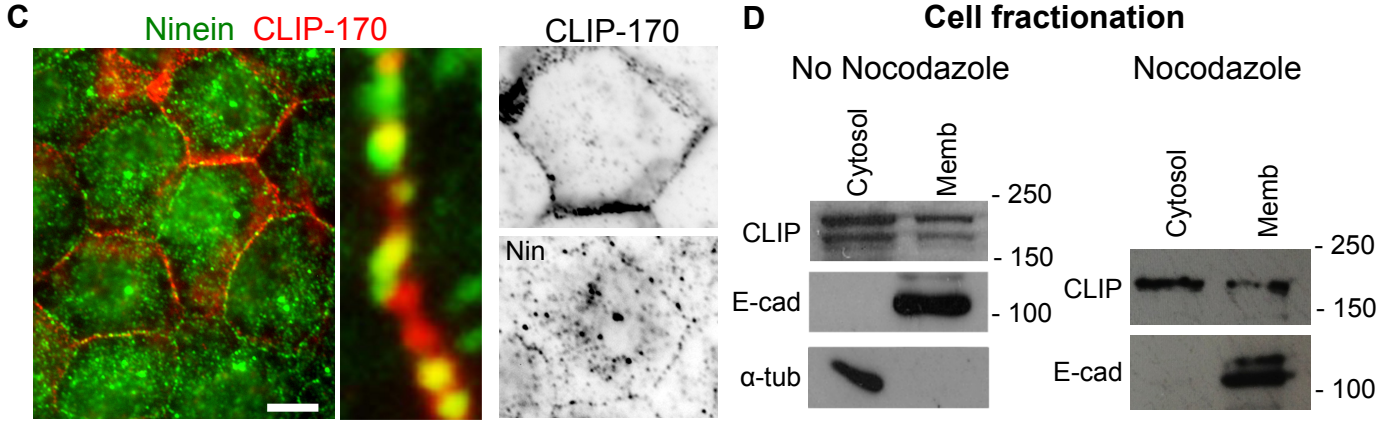

CLIP-170 and ninein in Nocodazole treated cells

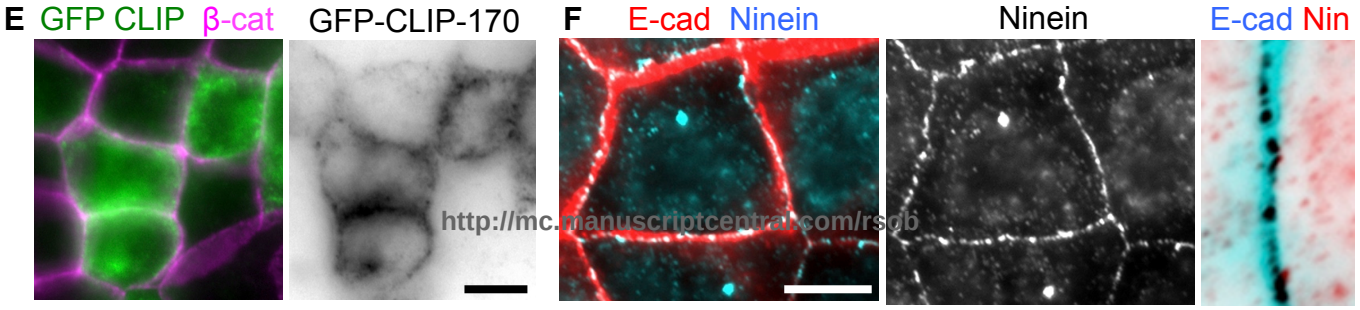

Fig.3

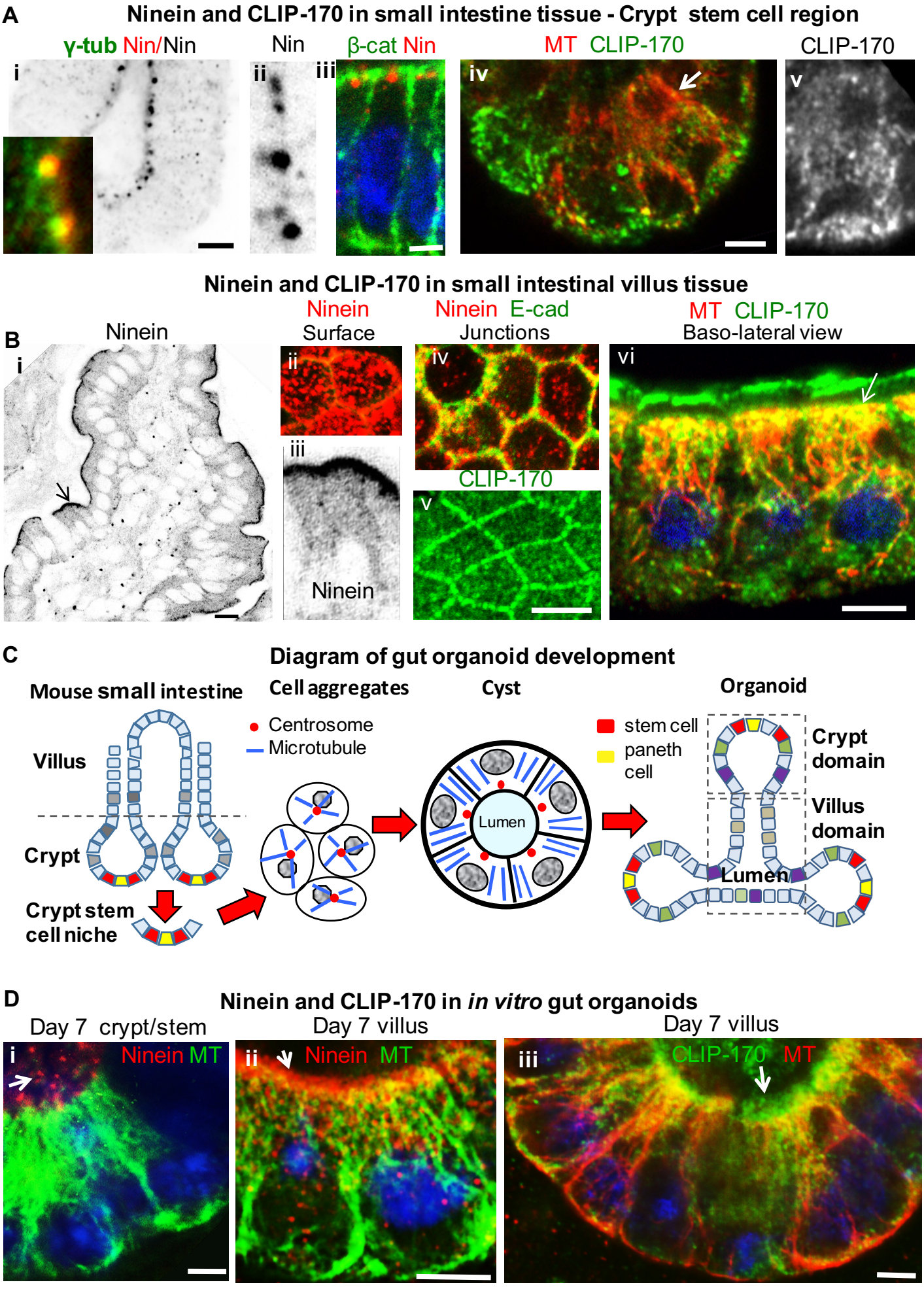
A
Ninein and CLIP-170 in small intestine tissue - Crypt stem cell region
γ-tub Nin/Nin
Nin
β-cat Nin
MT CLIP-170
CLIP-170
i
ii
iii
iv
v
Ninein and CLIP-170 in small intestinal villus tissue
B
Ninein
Ninein
Surface
Ninein E-cad
Junctions
MT CLIP-170
Baso-lateral view
i
ii
iii
iv
v
vi
CLIP-170
Ninein
C
Diagram of gut organoid development
Mouse small intestine
Cell aggregates
Cyst
Organoid
Centrosome
Microtubule
stem cell
paneth cell
Villus
Crypt
Crypt stem cell niche
Lumen
Crypt domain
Villus domain
Lumen
D
Ninein and CLIP-170 in in vitro gut organoids
Day 7 crypt/stem
Day 7 villus
Day 7 villus
i
Ninein MT
ii
Ninein MT
iii
CLIP-170 MT

Fig. 4 CLIP-170 siRNA depletion in MDCK cells and cortical ninein

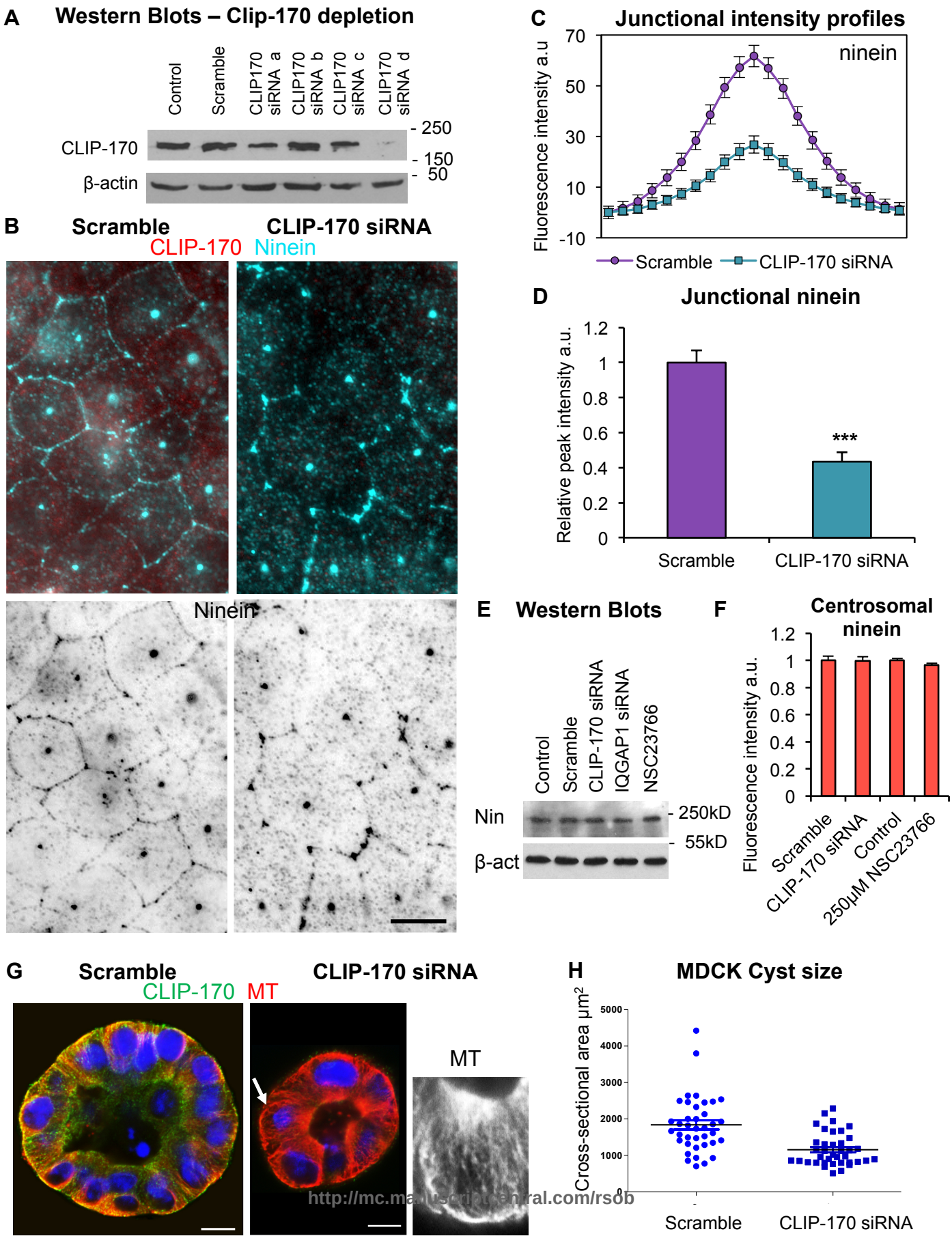

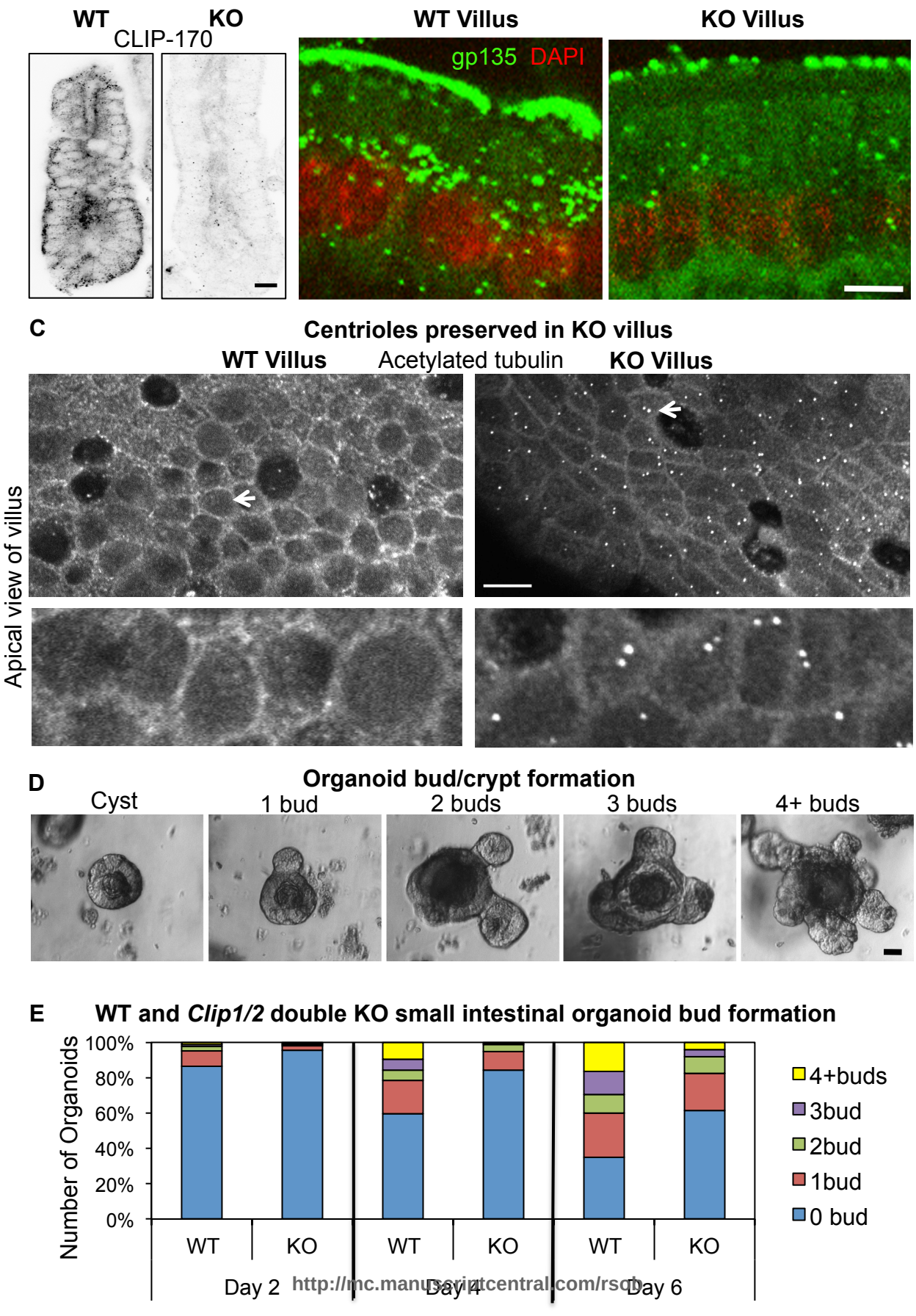
A. Isolated crypts
B. gp135 localises less efficiently to villus apex in KO
WT
KO
CLIP-170
WT Villus
KO Villus
gp135 DAPI
C
Centrioles preserved in KO villus
WT Villus
Acetylated tubulin
KO Villus
Apical view of villus
D
Organoid bud/crypt formation
Cyst
1 bud
2 buds
3 buds
4+ buds
E
WT and Clip1/2 double KO small intestinal organoid bud formation
Number of Organoids
100%
80%
60%
40%
20%
0%
WT
KO
WT
KO
WT
KO
Day 2
Day 4
Day 6
4+buds
3bud
2bud
1bud
0 bud

WT and *Clip1/Clip2* double knockout mouse intestinal tissue and organoids

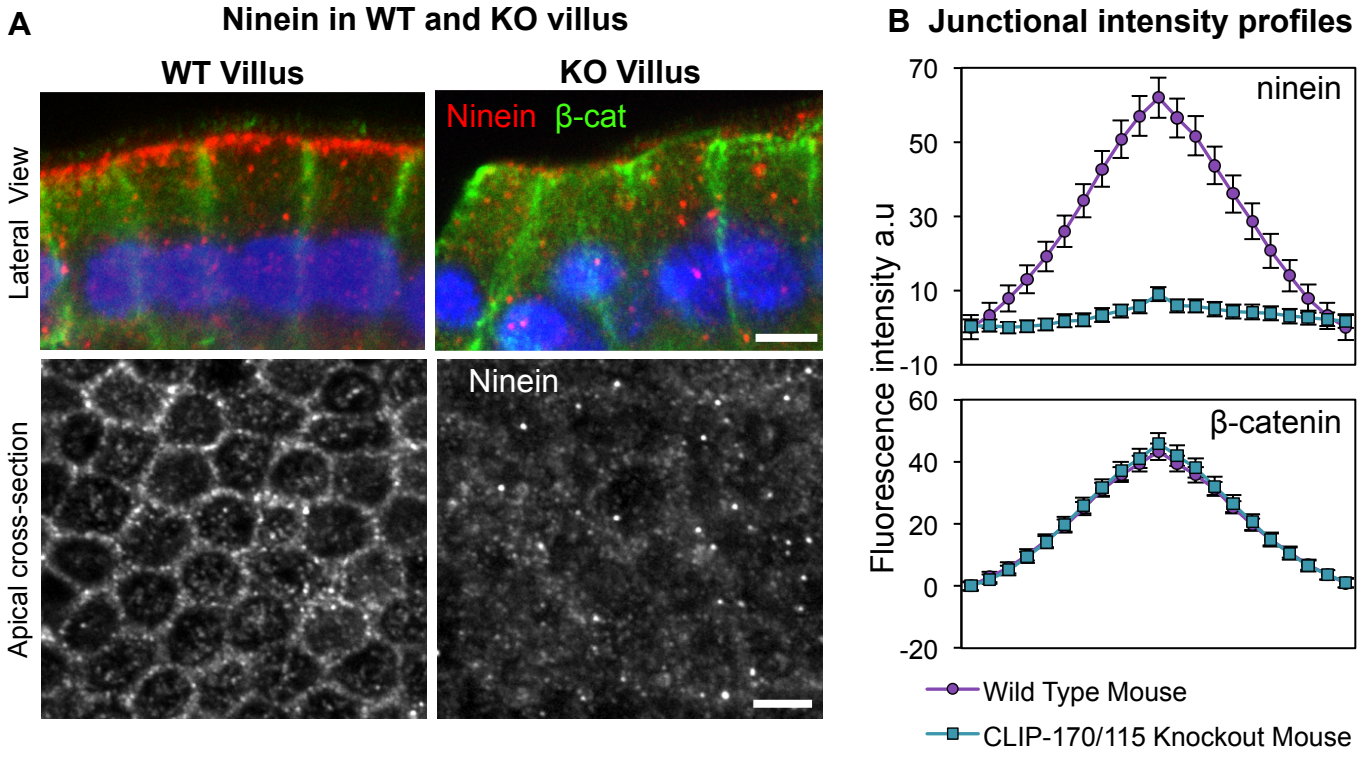

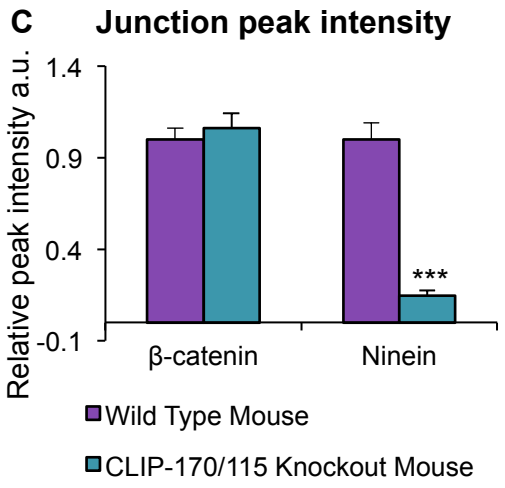

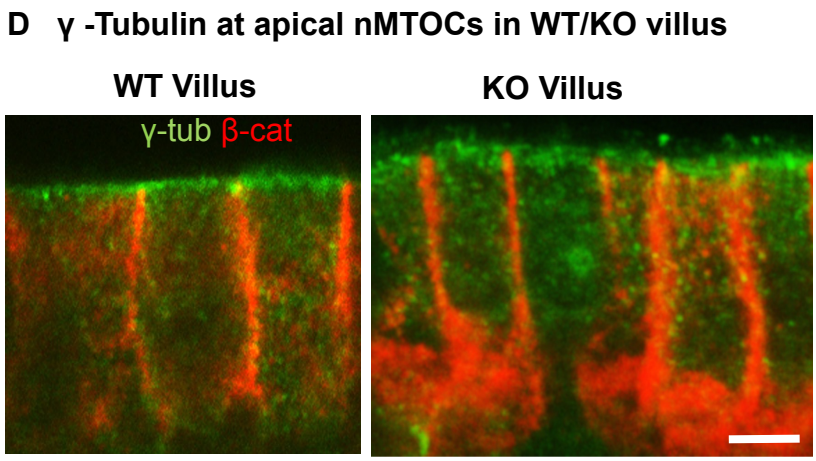

Fig. 7 CLIP-170 siRNA depletion and microtubule cortical targeting in ARPE-19 cells

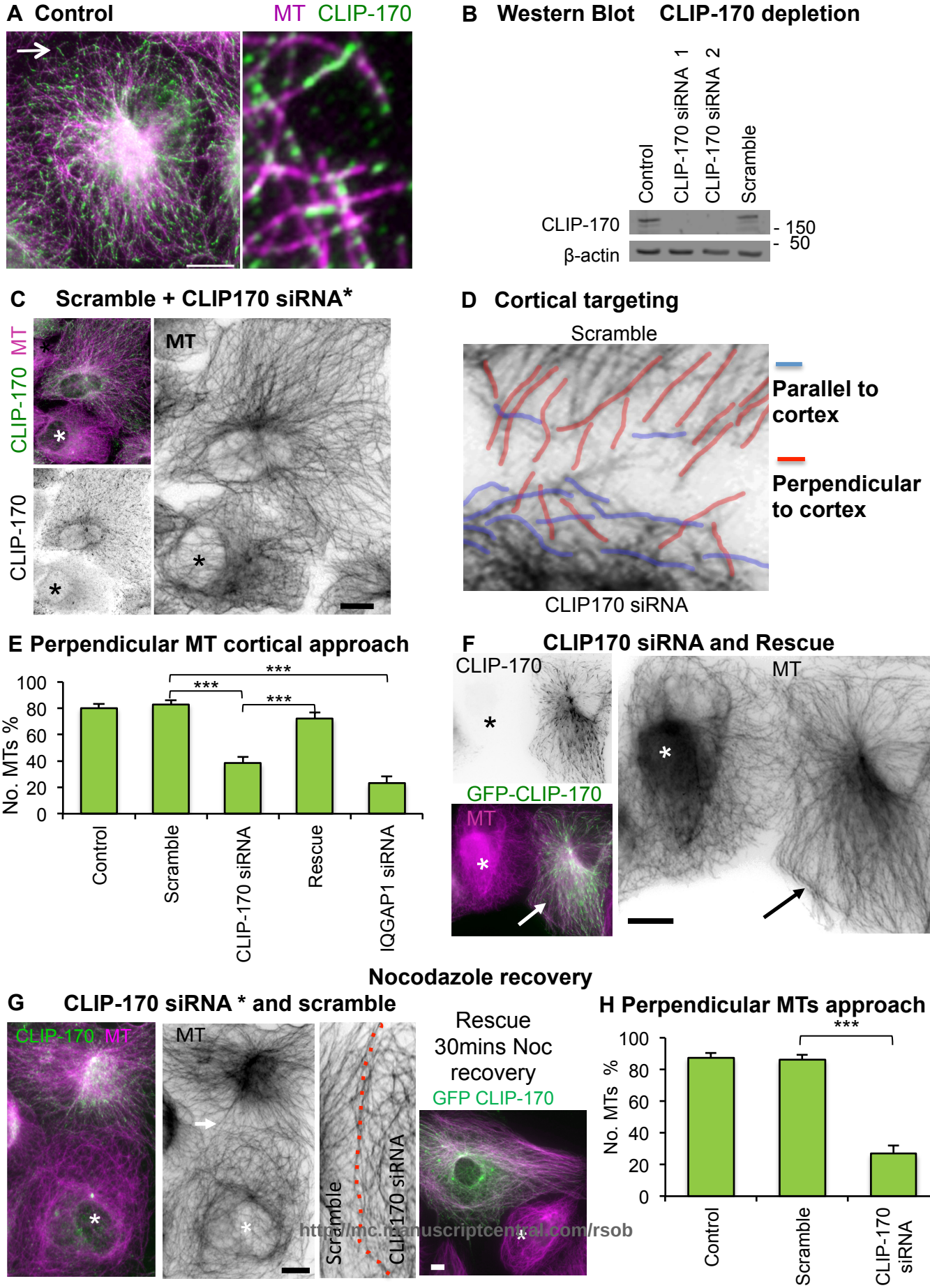

Submitted to Open Biology: FOR REVIEW ONLY

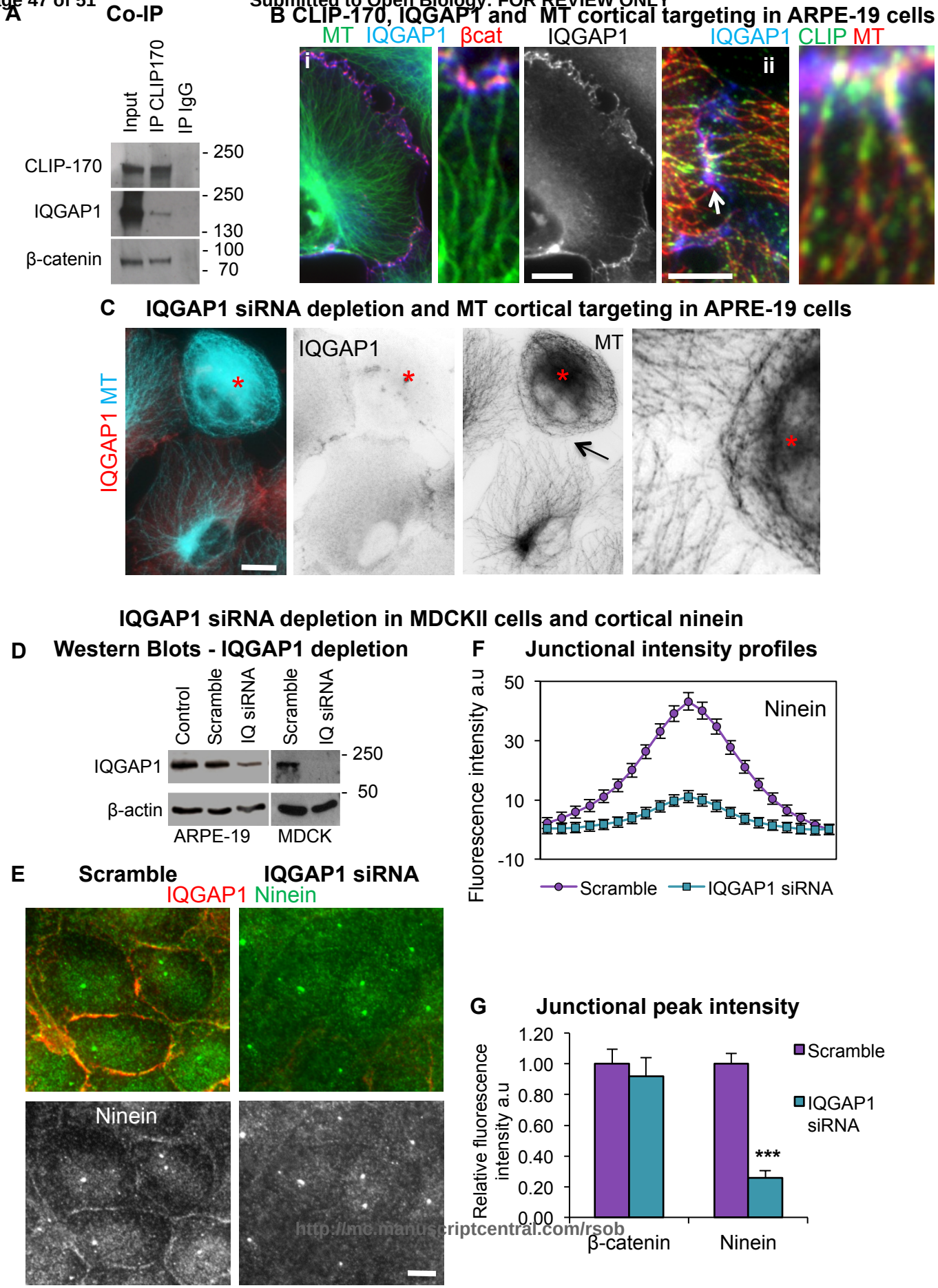

Rac1 inhibition in MDCKII cells and cortical ninein

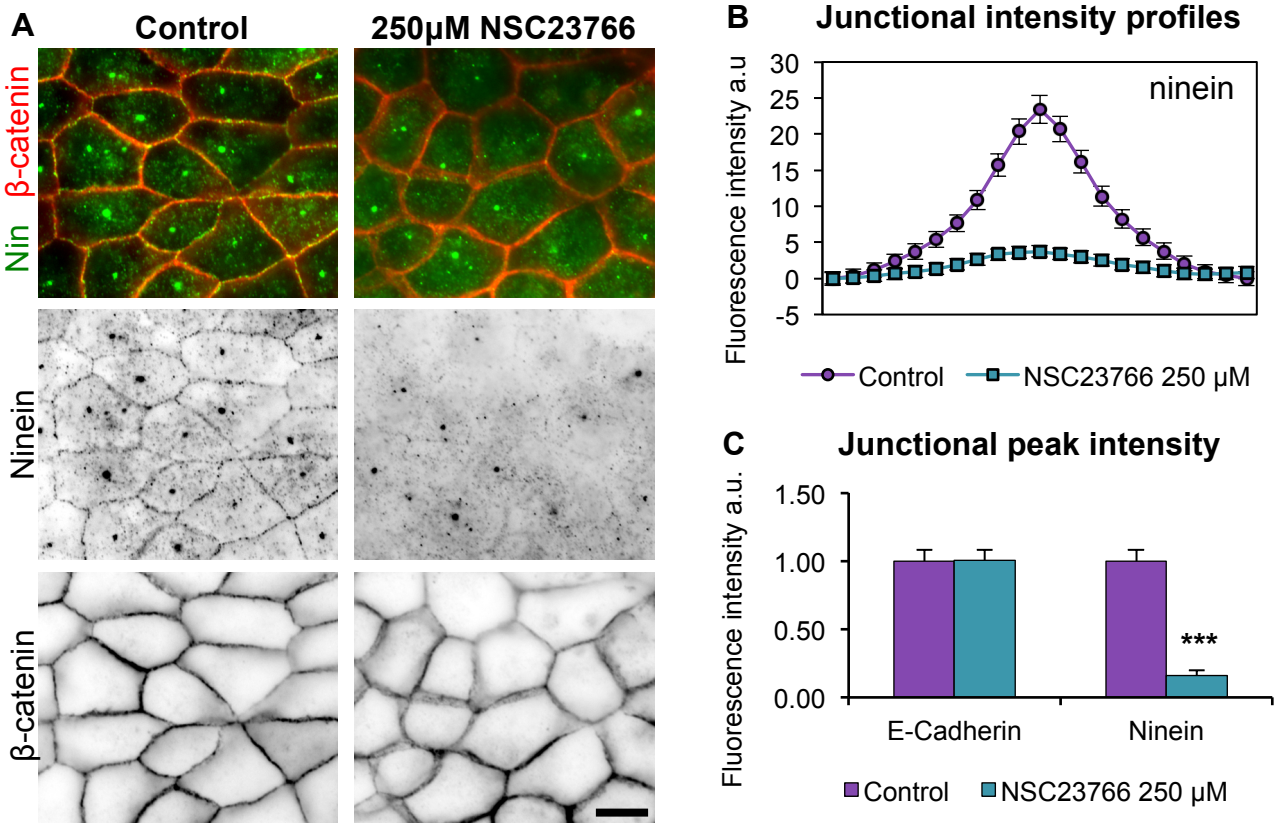

Rac1 inhibition and MT cortical targeting in APRE-19 cells

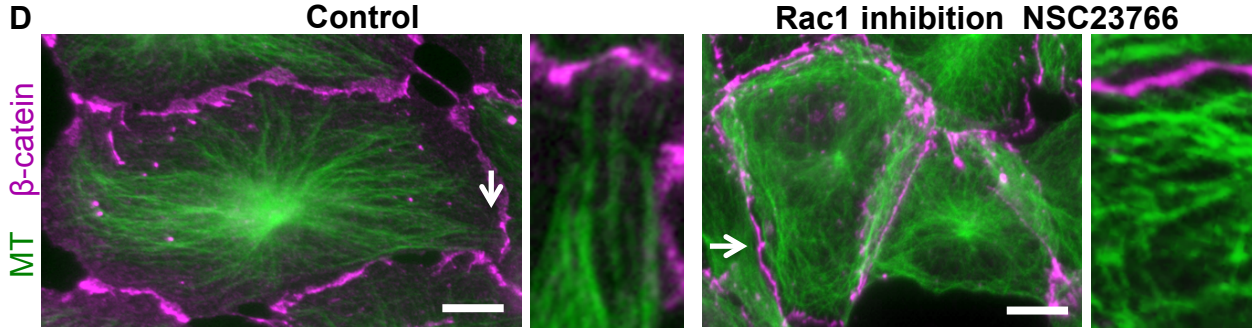

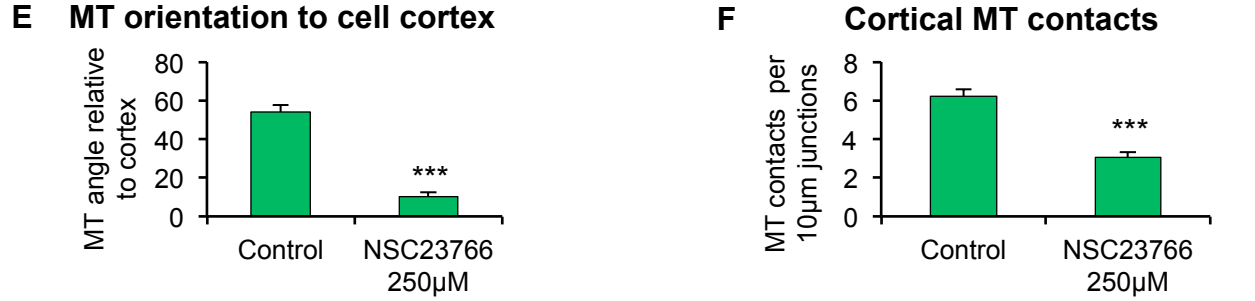

Fig. 10 Rac1 inhibition and CLIP-170 comets in ARPE-19 cells

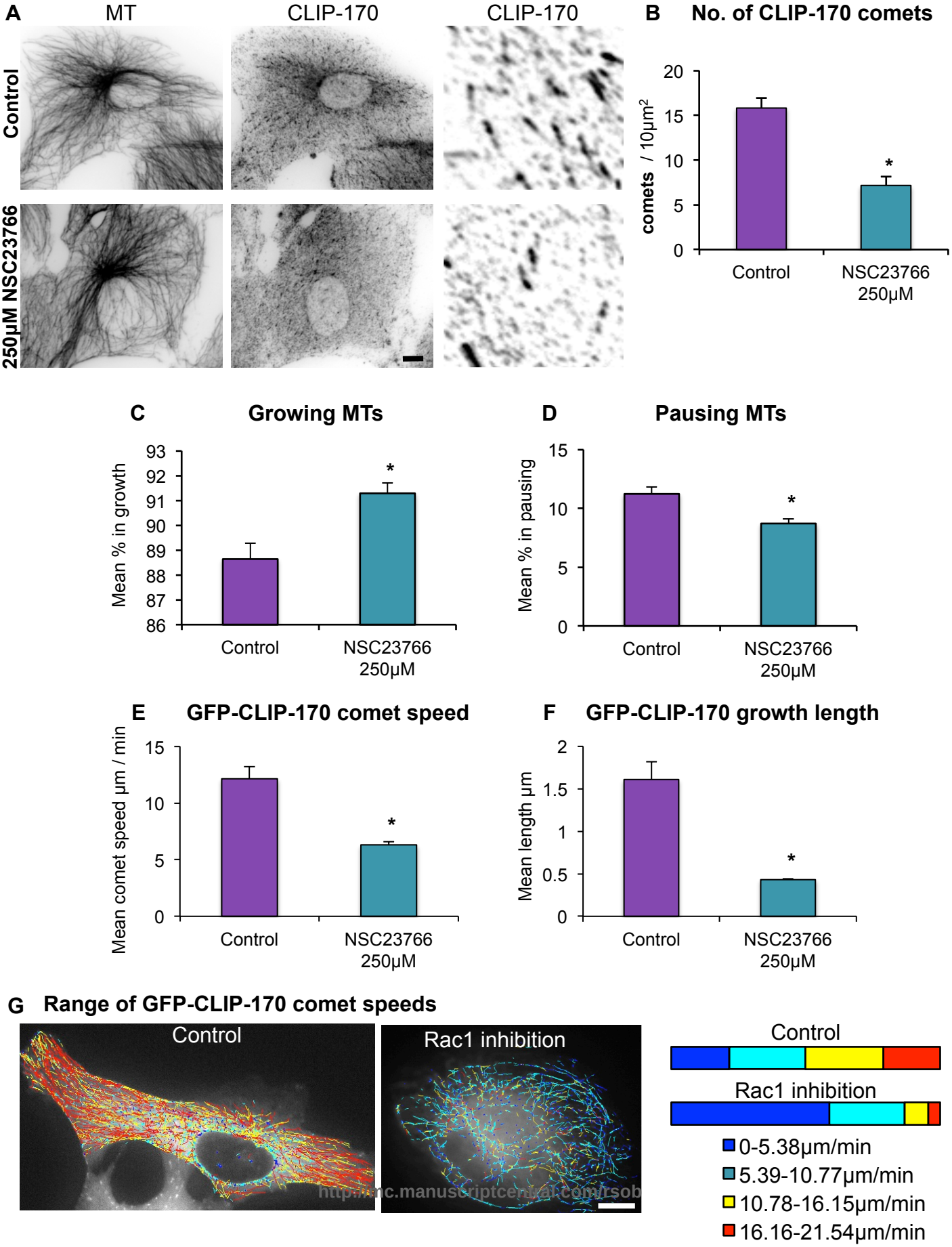

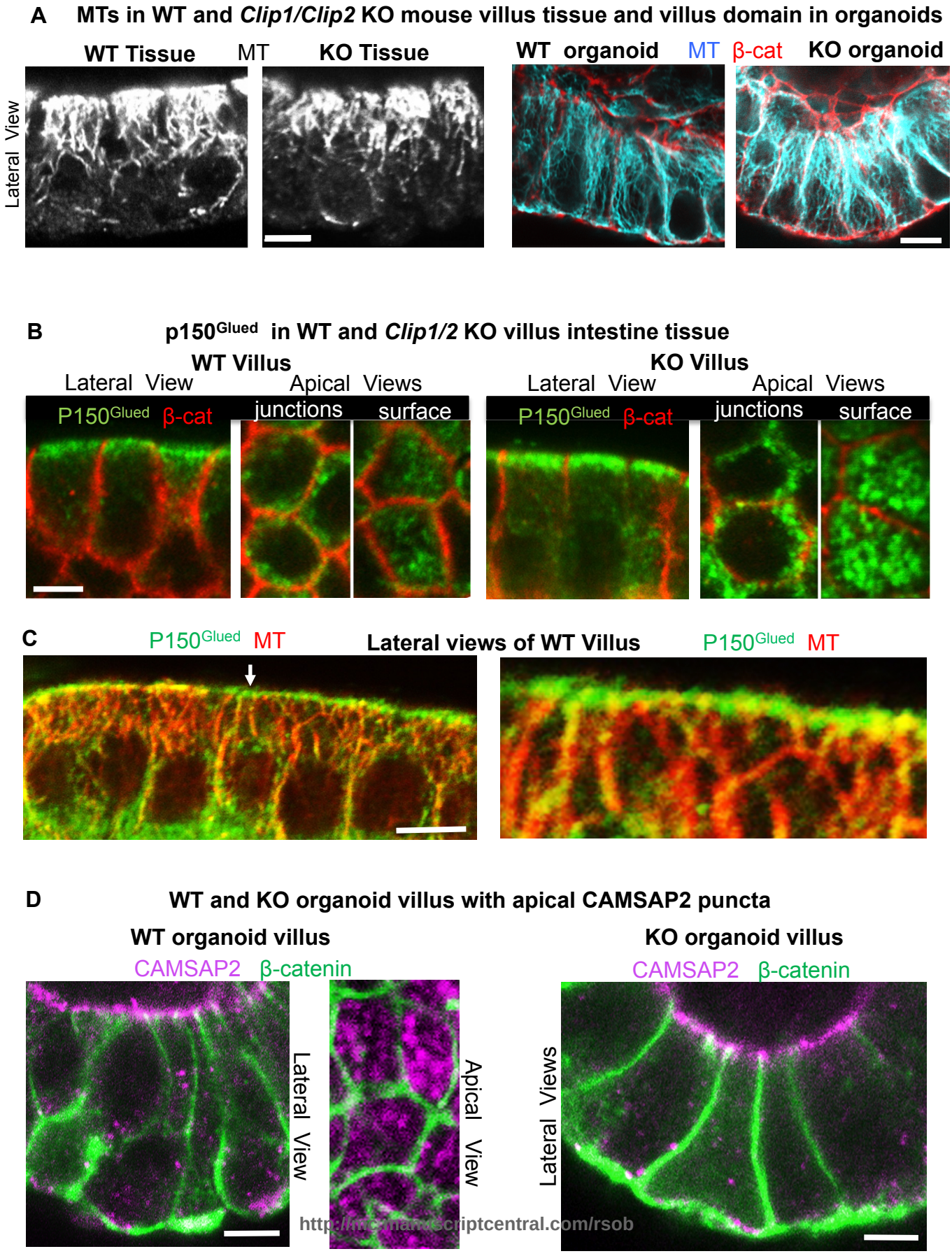

Fig. 12 Two models for ninein redeployment to n-MTOCs during epithelial differentiation

Model 1: CLIP-170 cortical targetting facilitates ninein delivery to n-MTOCs

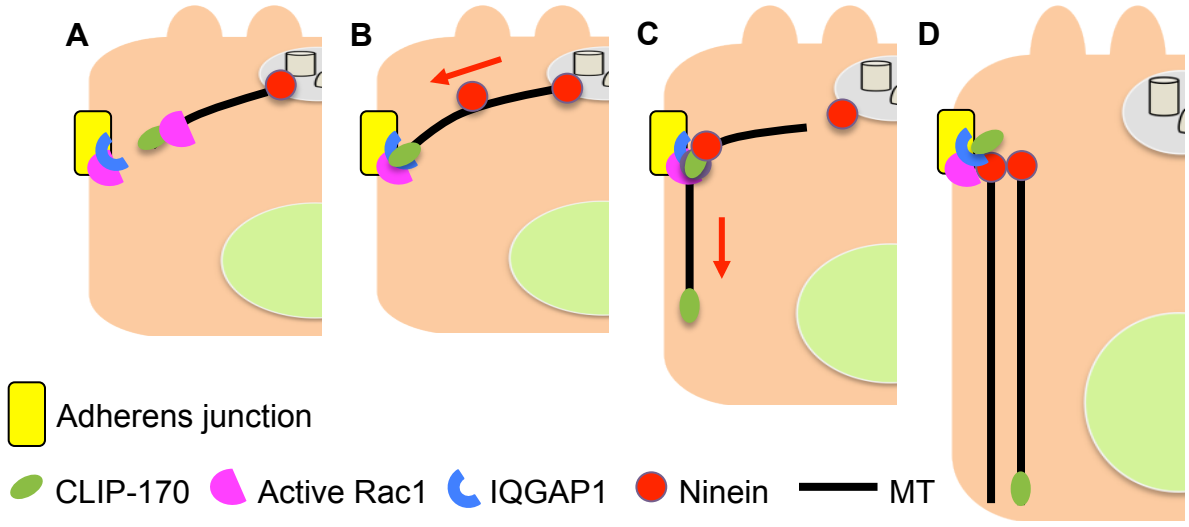

Model 2: Cortical CLIP-170, IQGAP1,Rac1 facilitates ninein recruitment to n-MTOCs